

IRIS FEATURE VECTOR REDUCTION USING HAAR WAVELET
TRANSFORM AND LOCAL BINARY PATTERN

By

Prajoy Podder

Student ID: 0416312017

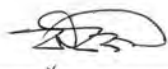
MASTER OF SCIENCE
IN
INFORMATION AND COMMUNICATION TECHNOLOGY

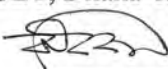



Institute of Information and Communication Technology
BANGLADESH UNIVERSITY OF ENGINEERING AND TECHNOLOGY
September, 2021

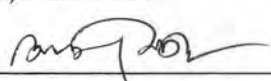
The thesis titled “**IRIS FEATURE VECTOR REDUCTION USING HAAR WAVELET TRANSFORM AND LOCAL BINARY PATTERN**” Submitted by Prajoy Podder, Roll No: 0416312017, Session: April-2016, has been accepted as satisfactory in partial fulfillment of the requirement for the degree of Master of Science in Information and Communication Technology on 19 September, 2021.


BOARD OF EXAMINERS

1. 

- Dr. Md. Rubaiyat Hossain Mondal
Professor
Institute of Information and Communication Technology
BUET, Dhaka-1205
- Chairman
(Supervisor)
2. 

- Dr. Md. Rubaiyat Hossain Mondal
Professor and Director
Institute of Information and Communication Technology
BUET, Dhaka-1205
- Member
(Ex officio)
3. 

- Dr. Md. Liakot Ali
Professor
Institute of Information and Communication Technology
BUET, Dhaka-1205
- Member
4. 

- Dr. Hossen Asiful Mustafa
Associate Professor
Institute of Information and Communication Technology
BUET, Dhaka-1205
- Member
5. 

- Dr. Sheikh Md. Rabiul Islam
Professor
Department of Electronics and Communication Engineering
Khulna University of Engineering & Technology (KUET)
Khulna, Bangladesh
- Member
(External)

CANDIDATE'S DECLARATION

It is hereby declared that this thesis/project or any part of it has not been submitted elsewhere for the award of any degree or diploma.



Prajoy Podder

DEDICATED TO MY PARENTS

Table of Contents

List of Figures	vii
List of Tables	ix
List of Abbreviations	x
List of Symbols	xii
Acknowledgement	xiii
Abstract	xiv
CHAPTER 1	1
Introduction	1
1.1 Biometrics	1
1.2 Motivation and Challenges	2
1.3 History	4
1.4 Proposed Approaches: Main Steps	5
1.5 Objectives of the thesis	8
1.6 Main Contribution of this Thesis	8
1.7 Thesis Organization	9
CHAPTER 2	11
Background Study	11
2.1 Biometric Overview	11
2.1.1 Requirements of Biological Systems	11
2.1.2 Biometric Systems	12
2.1.2.1 Verification Mode	12
2.1.2.2 Identification Mode	12
2.1.2.3 Modules in Biometric System	14
2.1.3 Biometric Devices	15
2.2 Iris Structure	16
2.2.1 Iris Features	17
2.2.1.1 The Crypts and Furrows	17
2.2.1.2 Freckles	18
2.2.1.3 ZigZag Collarette	18
2.3 Iris Recognition System Errors	19
2.4 Comparison of Iris Recognition with Other Biometrics	20
2.5 Strengths and Weakness of Iris Recognition	21
2.5.1 Strengths of Iris Recognition	21
2.5.2 Weakness of Iris Recognition	22
2.6 Application of Iris Recognition	22
2.7 Summary	24
CHAPTER 3	25
Iris Segmentation and Normalization	25
3.1 Overview	25
3.2 Image Acquisition	26
3.3 Literature Review	27
3.3.1 Hough Transform	27
3.3.2 Daugman's Integro-differential Operator	29
3.3.2 Eyelash and Noise Reduction	30

3.4 Morphology and Geometrical Approach Iris Localization	31
3.4.1 Inner and Outer Boundary Localization	31
3.5 Experimental Result of Segmentation Stage	37
3.6 Daugman’s Rubber-Sheet Model	39
3.6.1 Implementation	41
3.6.2 Enhancement of Normalization Image	42
3.6 Summary	43
CHAPTER 4	45
Feature Extraction using Three Level Haar Wavelet Transform and Modified Local Binary Pattern	45
4.1 Overview	45
4.2 Literature Review	46
4.3 The Proposed Feature Extraction Scheme	51
4.4 Summary	57
CHAPTER 5	58
LBPX: A Novel Feature Extraction Method for Iris Recognition	58
5.1 Overview	58
5.2 Literature Review	58
5.3 Methodology	60
5.4 Summary	62
CHAPTER 6	63
Matching and Distance Measurement	63
6.1 Overview	63
6.2 Hamming Distance	63
6.3 Experimental Results	65
CHAPTER 7	68
Experimental Result and Analysis	68
7.1 Overview	68
7.2 Datasets	68
7.2.1 Chinese Academy of Sciences - Institute of Automation (CASIA)	68
7.2.2 MMU	69
7.2.3 UBIRIS Database	70
7.3 Inner and Outer Boundary Detection	70
7.4 Performance Evaluation using Haar wavelet and MLBP	71
7.5 Performance Evaluation using LBPX:	74
CHAPTER 8	76
Conclusion and Future Works	76
8.1 Summary of the Work	76
8.2 Main Findings of the Work	76
8.3 Suggestions for Future Work	77
References	79

List of Figures

Fig. 1.1: Flow diagram of the proposed approach	7
Fig. 2.1: Block diagrams of enrollment, verification, and identification tasks are shown using the four main modules of a biometric system, i.e., sensor, feature extraction, matcher, and system database.	13
Fig. 2.2: Zigzag Collarett area localization from CASIA iris database	18
Fig. 2.3: Illustration of FAR	19
Fig. 2.4: Illustration of FRR	19
Fig. 3.1: Schematic diagram of image acquisition components	27
Fig. 3.2: (a) an eye image (020_2_1 from the CASIA database) (b) corresponding edge map (c) edge map with only horizontal gradients (d) edge map with only vertical gradients.	28
Fig. 3.3: Assuming r_{min} , r_{max} : (90, 110) the minimum and maximum values of the iris radius using Daugman's integrodifferential operator.	30
Fig. 3.4: The eyelash detection technique, eyelash regions are detected using thresholding and denoted as black	31
Fig. 3.5: Illustration of Iris localization steps according to the Morphology and Geometrical algorithm	34
Fig. 3.6: Flow Diagram of finding Pupil Center and its Boundary/Radius	36
Fig. 3.7: Location results for class I: (a) Daugman's method (b), Wildes' method, (c) Morphology and Geometrical approach	37
Fig. 3.8: Location results for class II: (a) Daugman's method (b) Wildes' method (c) Morphology and Geometrical approach	38
Fig. 3.9: Daugman's rubber sheet model	39
Fig. 3.10: Output of Normalization	40
Fig.3.11: Unwrapping Normalized Iris; CASIA [S1211L04]	42
Fig. 3.12: Unwrapping Normalized Iris; [S1211L05]	42
Fig. 3.13: Enhanced normalized image with the histogram	43
Fig. 4.1: Block diagram of the proposed approach for iris feature extraction.	52
Fig. 4.2: Three-level HWT	53
Fig. 4.3: Three-level wavelet decomposition of normalized iris	53
Fig. 4.4: Three-level HWT with the size of each level	54
Fig. 4.5: Center element of a 3x3 pixel image	56

Fig. 4.6: MLBP operation of 3x3 sub region: (a) the neighborhood of a pixel within the image, (b) the threshold version of the neighbourhood, (c) MLBP pattern where the middle pixel has been computed.	56
Fig. 6.1: An illustration of the shifting process.	65
Fig. 6.2: Unmatched Conditions	66
Fig. 6.3: Matched Condition	67
Fig. 7.1: Example iris images in CASIA-IrisV1	69
Fig. 7.2: Example iris images in CASIA-Iris-Interval	69
Fig.7.3: Example iris images in MMU1 Database	69
Fig. 7.4: Illustrations of (a, e, i) original input images; (b, f, j) images with inner and outer boundary detection; (c, g, k) segmented iris regions, (d, h, l) iris images after normalization	71
Fig. 7.5: (a) An original iris image from CASIA-IRIS-V4 dataset [84], (b) the final generated iris template, (c) larger view of the binarized template	72
Fig. 7.6: (a) An original iris image from CASIA-IRIS-V1 dataset [87], (b) the final generated iris template, (c) larger view of the binarized template	72
Fig. 7.7. (a) An original iris image from the MMU dataset [95], (b) the final generated iris template, (c) a larger view of the binarized template	73

List of Tables

Table 2.1: Comparison of different biometric security systems	20
Table 2.2: Cross-comparisons of different Biometric Products	22
Table 2.3: Template size of different biometrics	22
Table 3.1: Results obtained with the use of three methods for different classes	38
Table 3.2: Results obtained with the use of three methods for all images (CLR: correct location ratio)	38
Table 4.1: Summary of literature review	48
Table 7.1: Description of the datasets used in this work	72
Table 7.2: Comparisons of results with the existing methods	74
Table 7.3: Comparison of accuracy of proposed LBPX	75
Table 7.4: Comparative analysis between LBPX and other methods	75

List of Abbreviations

DWT: Discrete Wavelet Transform

HWT: Haar Wavelet Transform

HL: Horizontal Detail

VL: Vertical Detail

HH: Diagonal Detail

DFT: Discrete Fourier Transform

LBP: Local Binary Pattern

RIU: Rotation Invariant Uniform

CASIA: Chinese Academy of Sciences—Institute of Automation

ED: Euclidean Distance

NC: Normalized Co-relation

HD: Hamming Distance

FA: False Accept

FAR: False Accept Rate

FR: False Reject

FRR: False Reject Rate

ERR: Equal Error Rate

CRR: Correct Recognition Rate

CLR: Correct Location Ratio

ULBP: Uniform LBP

UIDAI: Universal Identification Authority of India

1D: One-Dimensional

2D: Two-Dimensional

PIN: Personal Identification Number

MMU: Multimedia University

IITD: IIT Delhi Iris Database

DoF: Degrees of Freedom

NIR: Near-Infrared

HT: Hough Transform

CHT: Circular Hough Transform

SI: Segmented Iris Image

NI: Normalized Iris Image

FWT: Fast Wavelet Transform

XOR: Exclusive OR

NFA: Number of False Acceptance

List of Symbols

Variable	Description
$\hat{i}(x, y)$	2D cepstrum with (x, y) representing quefrequency coordinates
$I(u, v)$	2D discrete-time Fourier Transform (DTFT)
$G_\sigma(r)$	smoothing function such as a Gaussian of scale σ
$F(U, V)$	2D DCT coefficient matrix
W	Angular Frequency
σ_x and σ_y	Standard deviations of x and y
x_c	The x-axis coordinate of the iris circle
y_c	The y-axis coordinate of the iris circle
R	The radius of the iris circle
g_c	Gray level of the center pixel, c
g_p	Gray level of the neighbouring pixel, p
$\psi_\oplus(s_p)$	Binary iris code obtained as XOR output
LBP_p	The MLBP operator
$LBP_{Q,R}^{ri}$	Rotation invariant LBP operator
$LBP_{Q,R}^{riu2}$	Rotation invariant uniform LBP operator

Acknowledgement

First of all, I would like to thank GOD for giving me the ability to complete this thesis work. I would like to express my sincere gratitude to my supervisor, Dr. Md. Rubaiyat Hossain Mondal, Professor and Director of IICT, BUET. This thesis would not have been completed without his support and guidance. I would like to express my great thanks and gratefulness for instructions, continuous encouragement, valuable discussions and careful review during the period of this research. I have learned many valuable lessons and concepts of Digital Image Processing from him through my study, which I have utilized to develop my abilities to work innovatively. His constant encouragement gave me the confidence to carry out my work.

I would also like to thank all the teachers and staff of IICT, BUET, for their cordial help and assistance during my study period.

Finally, I would like to thank my parents. Their unconditional support made it possible for me to finish this thesis.

Abstract

Iris recognition is a means of biometric identification. A key part of the recognition system using iris is the extraction of prominent texture information or features in the iris. The identification delay in iris recognition can be reduced by reducing the feature vector generated from the feature extraction of iris images. In this thesis, two algorithms are proposed for the reduction of the iris feature vector. The first method is the combination of Haar wavelet transformation (HWT) and local binary pattern (LBP) termed here as HWT-LBP. The second method is a new form of LBP termed LBPX. First, HWT-LBP is considered. In this case, input eye images are processed and converted to normalized iris images employing circular Hough transformation and Daugman's rubber sheet model. HWT is then applied to the normalized image. The output of this HWT goes through the LBP process. In this hybrid method, HWT is applied to the normalized iris image resulting in four output images, including the approximation image known as LL sub-band. This LL sub-band is then further decomposed using HWT into four sub-images. The resultant second-level LL is decomposed using HWT into the third-level LL sub-band. The application of repeated HWT extracts the major information containing region, reducing the information size. Next, MLBP is applied to the obtained LL, where MLBP includes LBP and XOR operations. The output of MLBP is a binary iris template. The effectiveness of this proposed hybrid HWT-MLBP method is experimentally evaluated using three different datasets, namely CASIA-IRIS-V4, CASIA-IRIS-V1 and MMU. The proposed HWT-MLBP method can obtain a reduced feature vector length of 1×64 . For instance, when applied to CASIA-IRIS-V1 dataset, HWT-MLBP can obtain an average correct recognition rate of 98.30% and false acceptance rate of 0.003%. Results indicate that the proposed HWT-MLBP outperforms existing methods in terms of reduced feature length, which ensures faster iris recognition. Next, the LBPX method is considered. The LBPX method is based on the concepts of uniform LBP, rotation-invariant LBP, and XOR operators. Moreover, the existing rotation-invariant uniform LBP (RIU LBP) method is applied here in the context of iris feature extraction. LBPX is applied to the normalized iris images. The performance of LBPX based recognition system adopting iris image is evaluated in terms of accuracy and feature vector length. This is done for three datasets CASIA-

IRIS-V4, UBIRIS and IITD. Results indicate that LBPX can achieve acceptable accuracy values of 97.15%, 97.20%, 96% and 96.40% for CASIA-IRIS-V1, CASIA-IRIS-V4, UBIRIS, and IITD datasets, respectively. Furthermore, results show LBPX outperforms existing feature extraction methods in terms of reduced feature-length, ensuring faster iris recognition.

CHAPTER 1

Introduction

1.1 Biometrics

The requirement for a reliable and secure authentication system is extremely important since security and personal authentication are increasingly needed because of the new dimension in the security problems faced by the globe today. Biometric identification methods are quite popular because they can verify people through their unique and measurable personal traits that are harder to alter or counterfeit [1-6]. The constant hacking into organizational and personal systems and the raging identity robbery experienced today in the world is proof of an obsolete and technologically advanced world of the traditional authentication systems based on key codes, passwords and tokens. Iris biometrics, a relatively new biometric technology in comparison to other biometric technologies, has been quite popular among computer vision and pattern recognition scientists because of certain key factors: i) the iris is an internal body organ that can be captured without invasion employing a cheap CCD camera, ii) the iris is considered to be one of today's best biometrics, and it is highly unique for the individual that the iris patterns are completely different from both the single iris and identical twins [4-8]. These fascinating features of the iris have spurred studies on the use of iris for the identification of persons.

However, identification of iris entails complicated mathematical procedures, often too slow to be applied in highly demanding and advanced systems today. Furthermore, the capture process of most installed iris recognition systems is not very convenient and may result in a loss of time. In addition, the environment for capturing iris pictures involves the employment of near-infrared lighting to highlight the iris before capture, a source of the mistake, and a requirement for the full cooperation of the person. These are restrictive variables for iris biometrics. Today, new research has begun to push the frontiers of iris biometrics and the capturing of the iris in motion and is increasing at a distance. Those new iris capturing technologies are now producing un-ideal iris pictures that are more difficult to analyze utilizing the traditional iris biometric algorithm. Non-ideal iris pictures include camera noise, reflections, and occlusions. The extraction of the iris part from the eye picture, or

more broadly a segmentation of the iris portion in the eye image, is a highly crucial operation for any iris recognition system as it specifies the portion of the iris image utilized for the identification of the iris. The diverse nature of the iris pictures may be an extremely hard operation. The extraction of significant iris characteristics utilized to depict the iris sample is likewise very difficult due to its richness and complexity. A novel method for iris detection achieving these tasks is presented in this work and is evaluated to establish their efficacies.

1.2 Motivation and Challenges

The amazing uniqueness of iris patterns and the ability to record iris photography in a non-invasive way have motivated biometrics researchers to build an automatic iris identification system based on 2-D iris pictures. Although there has been a well-documented performance of existing iris recognition systems, the problem of reaching high accuracy in non-ideal pictures with the efficiency of the iris remains a difficulty without an effective solution. The efficiency of iris recognition systems depends heavily on the precision and speed of the iris segmentation module. The improvement of the speed and precision of the segmentation module would, therefore, substantially improve the efficiency and efficacy of the iris identification system. In non-ideal iris picture segmentation, the iris borders are either divided into an expensive evolutionary curve approach based on a level method [9] or a supervised way of learning. Both approaches are costly and have a detrimental influence on the overall system speed.

In addition, extracting significant characteristics from the non-ideal iris sample remains an issue to be solved. Current iris extraction methods describe the sample of iris with a high dimensional iris code that affects the effectiveness of categorization. In addition, with poorer quality pictures of iris recorded in the course of the day under no subject, existing iris extraction algorithms mainly lead to a lot of erroneous rejection mistakes. The representation of the iris with smaller iris codes is, therefore, a topic that has yet to be investigated without an effective answer. Most contemporary methods for iris feature extraction and representation have tried to use discrete wavelets to extract iris features [6, 10, 11]. This approach is normally affected by shift variance and phase problems which are inherent in discrete wavelet transform (DWT). A new system must be built to overcome these obstacles and to build a more efficient

and accurate iris segmentation and display approach, which is our motivation in this research. Furthermore, the success of iris recognition is our greatest motivation in various critical areas of application, including home security, border and security surveillance, web security, national identity management, fast passenger information management, controlled access to privileged information, forensic inquiry, and welfare management. The broad scope of the use of iris biometrics, therefore, means that this study will be of great advantage to many organizations, governments and people alike.

Most of the current research on iris recognition mainly focused on iris segmentation schemes, which are usually based on the complete information of the iris region. In this thesis, the iris segmentation approach has been emphasized based on computation time locating the iris area. In order to improve time efficiency, the Morphological segmentation approach has been used to speed up the process of locating the iris area. The traditional approach of iris recognition spends considerable computation time locating the iris area. In this thesis, a feature selection strategy using the fusion of Haar wavelet decomposition and extension of local binary pattern analysis is proposed for dimensional reduction as well as to minimize recognition error. Furthermore, the Hamming distance method is utilized for matching proposes.

The primary challenges confronting iris recognition systems are as follows:

- (i) Lack of robustness: The excellent recognition accuracy reported by most contemporary iris recognition algorithms in highly limited imaging conditions can simply be depleted when the same algorithm is used in an unconstrained setting. It is quite straightforward to produce an amazing performance with a low error rate in a severely limited imaging environment when a high-quality iris picture is acquired utilizing a sophisticated imagery setup [8, 12-19]. Most existing state-of-the-art iris recognition algorithms, on the other hand, fail when used in a less cooperative iris capture situation, when the chances of acquiring a low-quality iris image are extremely high. Iris images are taken utilizing a flexible imagery setup in an uncontrolled imaging environment, and as a result, noises such as motion blur, camera diffusion, head rotation, gaze direction, camera angles, reflections, low contrast, brightness, occlusions, and pupil dilation are common [20-22]. These non-idealities significantly affect

the performance of both the iris segmentation and feature representation algorithms, and as a result, the iris recognition algorithm's overall performance suffers.

- (ii) Iris and pupil boundary non-circularity: Researchers have discovered that the iris and pupil boundaries have arbitrary shapes [23, 24]. As a result, if fitted with some relatively basic forms like circles or ellipses, this can result in segmentation mistakes. The precise delineation of the iris' limits has remained a problem to this day.
- (iii) Speed: The current time efficiency of modern iris recognition technologies restricts the use of iris biometrics in today's high-demand, high-speed systems. Iris segmentation is regarded as the bottleneck in iris recognition systems because it takes the longest time to complete [24, 25].
- (iv) Dimensionality: The millions of interclass and intraclass comparisons that occur during iris recognition contribute to iris biometric systems' time inefficiency. The high dimensionality of the recognition system increases the number of interclass and intraclass comparisons made at the classification level, slowing down total recognition speed. As a result, it is necessary to minimize the dimensionality of the iris feature vector while keeping high accuracy.

In light of these challenges, it is pertinent that a new iris segmentation algorithm with enhanced performance and efficiency is developed to meet today's needs. Moreover, this research work looks at reducing the dimensionality of the iris feature vector through a feature selection technique. In order to improve the speed of the recognition system, a method is developed for selecting the most prominent features of the iris for iris representation which reduces the dimensionality of the iris feature vector and improves speed.

1.3 History

Dr. Leonard Flom and Aron Safir's 1980s work on iris recognition resulted in the first general idea patent. However, John Daugman, pioneered the utility of iris recognition as a means of human verification, as well as the algorithms that build a digital

representation of the iris pattern and enable the matching of one iris to another identified via a thorough search of even very large databases. Although John Daugman invented and patented the first algorithms for performing iris recognition, as well as the earliest articles and live demonstrations, the notion underlying his discovery dates back considerably further. The basic theoretical concept underlying Daugman's methods is that the failure of a statistical independence test can provide an extremely strong basis for pattern identification. He patented this method of iris recognition and the underlying Computer Vision algorithms for image processing, feature extraction, and matching in 1994 and published the paper [1]. These pioneering algorithms have been widely licensed by a number of firms (IriScan, Iridian, Sarnoff, Sensor, LG-Iris, Panasonic, Oki, BI2, IrisGuard, Unisys, Sagem, Enschede, Securimetrics, and L1. With numerous advancements over the years, these algorithms remain the foundation for all important public iris recognition implementations today. However, scholarly study on numerous elements of this technology has blossomed in recent years. As Bowyer et al. stated in their survey, over 1,000 articles have been published in the previous few years on optics, photonics, sensors, biology, genetics, ergonomics, interfaces, decision theory, coding, compression, protocol, security, hardware, and algorithmic elements of this technology. However, the most astounding deployment began in 2011 in India, where the government is registering the iris patterns (and other biometrics) of all 1.2 billion individuals in the Aadhaar scheme for entitlement distribution, which is administered by the Universal Identification Authority of India (UIDAI). Its objective is to provide each person with a biometrically verifiable unique entitlement number (Aadhaar) via which benefits can be claimed and social inclusion is improved; thus, the slogan of UIDAI is: "To give the poor an identity".

1.4 Proposed Approaches: Main Steps

An Iris recognition method is proposed with a feature vector size-reduction scheme based on Haar wavelet and LBP. Fig. 1.1 illustrates the main steps of the proposed approach. In the image pre-processing stage, iris and pupil boundary are detected by contact labelling of binary image and basic geometrical principles. Eyelashes and other non-iris regions are eliminated using wavelets and thresholding methods. For avoiding the size inconsistencies of the localized region, the annular iris part is

normalized into a rectangular block. Haar wavelet decomposition and LBP are applied to extract the discriminant iris features from the normalized area and reduce the dimension of the feature vector. After that, a conventional approach of Hamming distance is used for iris pattern classification.

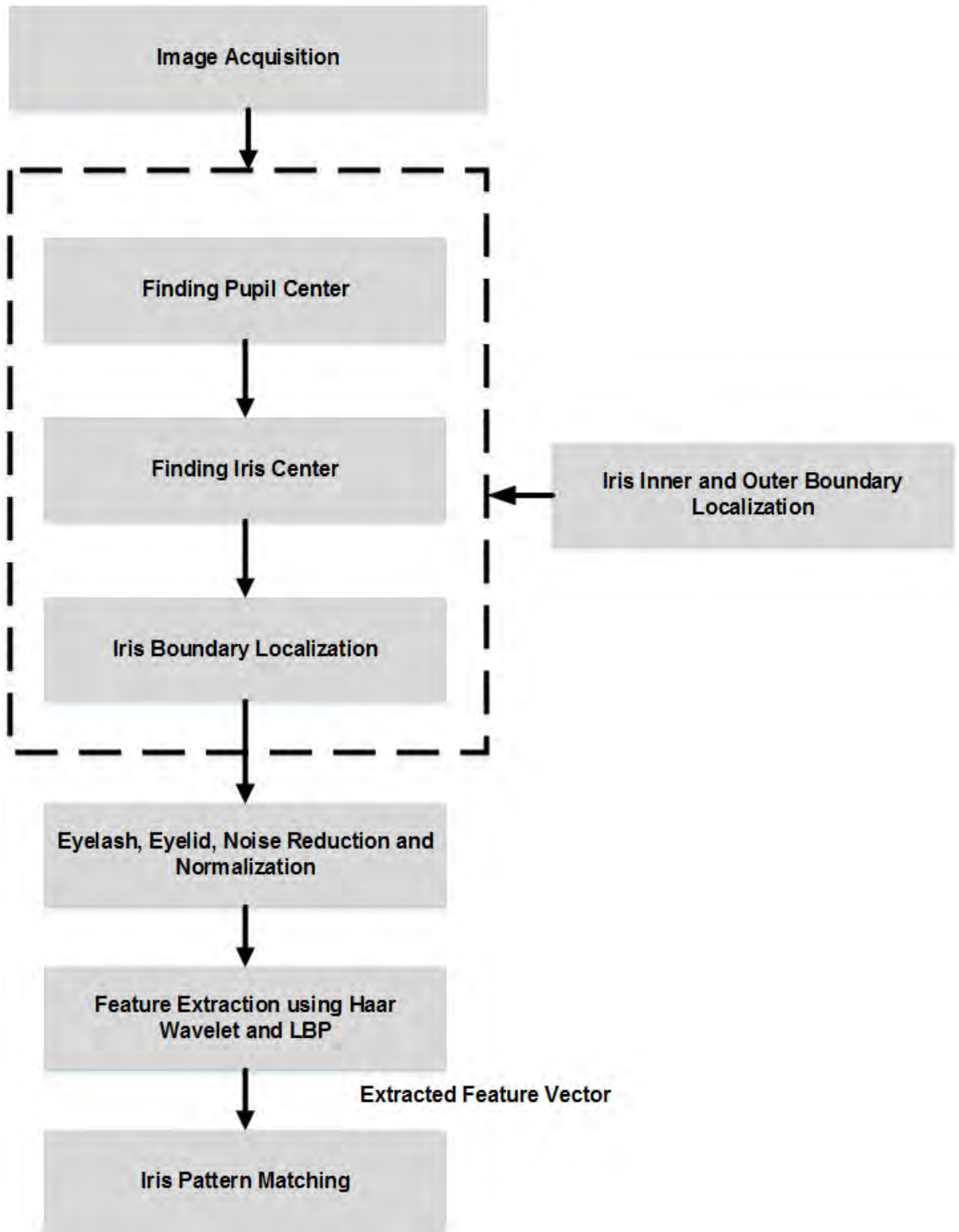


Fig. 1.1: Flow diagram of the proposed approach

1.5 Objectives of the thesis

The objectives of this research work are listed as follows:

- a) Familiarization with biometric systems.
- b) Iris Segmentation with Eyelids, eyelashes and noise detection to increase the recognition accuracy in subsequent processing.
- c) Normalizing the localized or segmented iris region to avoid the size inconsistencies
- d) Reducing the size of the iris feature vector with a new hybrid feature extraction method.
- e) Performance evaluation of a proposed approach for reducing the size of an iris feature vector.
- f) Reducing the feature length without loss of major information.
- g) Performance evaluation of Hamming distance as matching purposes.

1.6 Main Contribution of this Thesis

The main contributions are enlisted as follows:

- (i) A new hybrid iris feature extraction method is proposed. This new method is based on repeated *Haar wavelet transformation* (HWT) and MLBP. Note that MLBP is the local binary pattern (LBP) operation followed by Exclusive OR (XOR). This proposed method is different from the technique used single-level HWT and LBP (without XOR) in the context of face recognition.
- (ii) A novel iris feature extraction method termed here as local binary pattern X (LBP X) is proposed in this paper. This new method is based on the concepts of uniform LBP, rotation-invariant LBP, and XOR operators.

Moreover, the existing rotation-invariant uniform LBP (RIU LBP) method, reported earlier for face recognition, is applied here in the context of iris feature extraction.

- (iii) The efficacy of the HWT-MLBP method is evaluated using three well-known benchmark datasets: CASIA-Iris-V4, CASIA-Iris-V1, and MMU iris database. Next, the effectiveness of the LBPX method is evaluated using CASIA-IRIS-V4, UBIRIS, and IITD datasets.
- (iv) A comparison is made of the new techniques with the existing methods of feature extraction in terms of feature vector length, FAR, and FRR.

1.7 Thesis Organization

The thesis is organized into eight chapters. An overview of these chapters is presented below.

- Chapter 1 introduces the main motivation and contribution of this thesis work and gives the objectives.
- Chapter 2 describes a background study of biometric authentication and verification system with detailed concepts of iris features and its advantage over other biometric modules.
- Chapter 3 describes iris recognition approaches and system design. This chapter also explains iris image acquisition, image preprocessing, segmentation procedure, and the flow diagram of the proposed method for iris boundary localization. This chapter also includes normalized iris images of different iris databases after implementing the unwrapping algorithm.
- Chapter 4 explains a novel feature extraction method proposed for faster iris recognition. This new method is based on repeated Haar wavelet transformation (HWT) and MLBP. The application of repeated HWT extracts the major information-containing region reducing the information size. MLBP is the local binary pattern (LBP) operation followed by XOR.

- Chapter 5 describes a new iris feature extraction method called local binary pattern X (LBP X). This new method is based on the concepts of uniform LBP, rotation-invariant LBP, and XOR operators. Moreover, the existing rotation-invariant uniform LBP (RIU LBP) method, reported earlier for face recognition, is applied here in the context of iris feature extraction.
- Chapter 6 explains some distance measurement parameters to measure the closeness of two iris templates. A decision threshold is applied to differentiate the genuine and imposter scores.
- Chapter 7 explains different iris databases used for this thesis work. This chapter also explains the analysis of experimental result and compare them with other methods.
- Finally, the conclusion and future scope of iris recognition system biometric security application are described.

CHAPTER 2

Background Study

2.1 Biometric Overview

Any automatically measurable, robust, and distinctive physical characteristic or personal trait that can be used to identify an individual or verify the claimed identity of an individual is called Biometrical Identification or simply Biometrics. It's a combination of two Greek words: Bios means Life, and Metrics means To Measure.

2.1.1 Requirements of Biological Systems

Any human physiological and/or behavioural characteristic can be used as a biometric characteristic as long as it satisfies the following requirements:

- a) Universality: each person should have the characteristic;
- b) Distinctiveness: any two persons should be sufficiently different in terms of the characteristic;
- c) Permanence: the characteristic should be well invariant (concerning the matching criterion) over some time;
- d) Collectability: the characteristic can be measured quantitatively.

However, in a practical biometric system (i.e., a system that employs biometrics for personal recognition), there are several other issues that should be considered, including:

- a) Performance, which refers to the achievable recognition accuracy and speed, the resources required to achieve the desired recognition accuracy and speed, as well as the operational and environmental factors that affect the accuracy and speed;
- b) Acceptability, which indicates the extent to which people are willing to accept the use of a particular biometric identifier (characteristic) in their daily lives;

- c) Circumvention, reflects how easily the system can be fooled using fraudulent methods.

2.1.2 Biometric Systems

A biometric system is simply a pattern recognition system that functions by receiving biometric data from a person, extracting a feature set from the obtained data, and comparing this feature set to the template set in the database. A biometric system may function in either verification or identification mode, depending on the application environment.

2.1.2.1 Verification Mode

In the verification mode, the system confirms a person's identification by comparing the collected biometric data to her own biometric template(s) stored in the system database. In such a system, a person who wants to be recognized claims an identity, usually through a PIN (Personal Identification Number), a user name, a smart card, or other means, and the system performs a one-to-one comparison to determine whether the claim is true or not (refer to Fig. 2.1). Identity verification is commonly used for positive recognition to prevent several persons from using the same identity.

2.1.2.2 Identification Mode

In the identification mode, the system recognizes an individual by searching the templates of all the users in the database for a match. Therefore, the system conducts a one-to-many comparison to establish an individual's identity without the subject having to claim an identity. Identification is a critical component in negative recognition applications where the system establishes whether the person is who she (implicitly or explicitly) denies being.

Identification may also be used in positive recognition for convenience (the user is not required to claim an identity). While traditional methods of personal recognition such as passwords, PINs, keys, and tokens may work for positive recognition, negative recognition can only be established through biometrics.

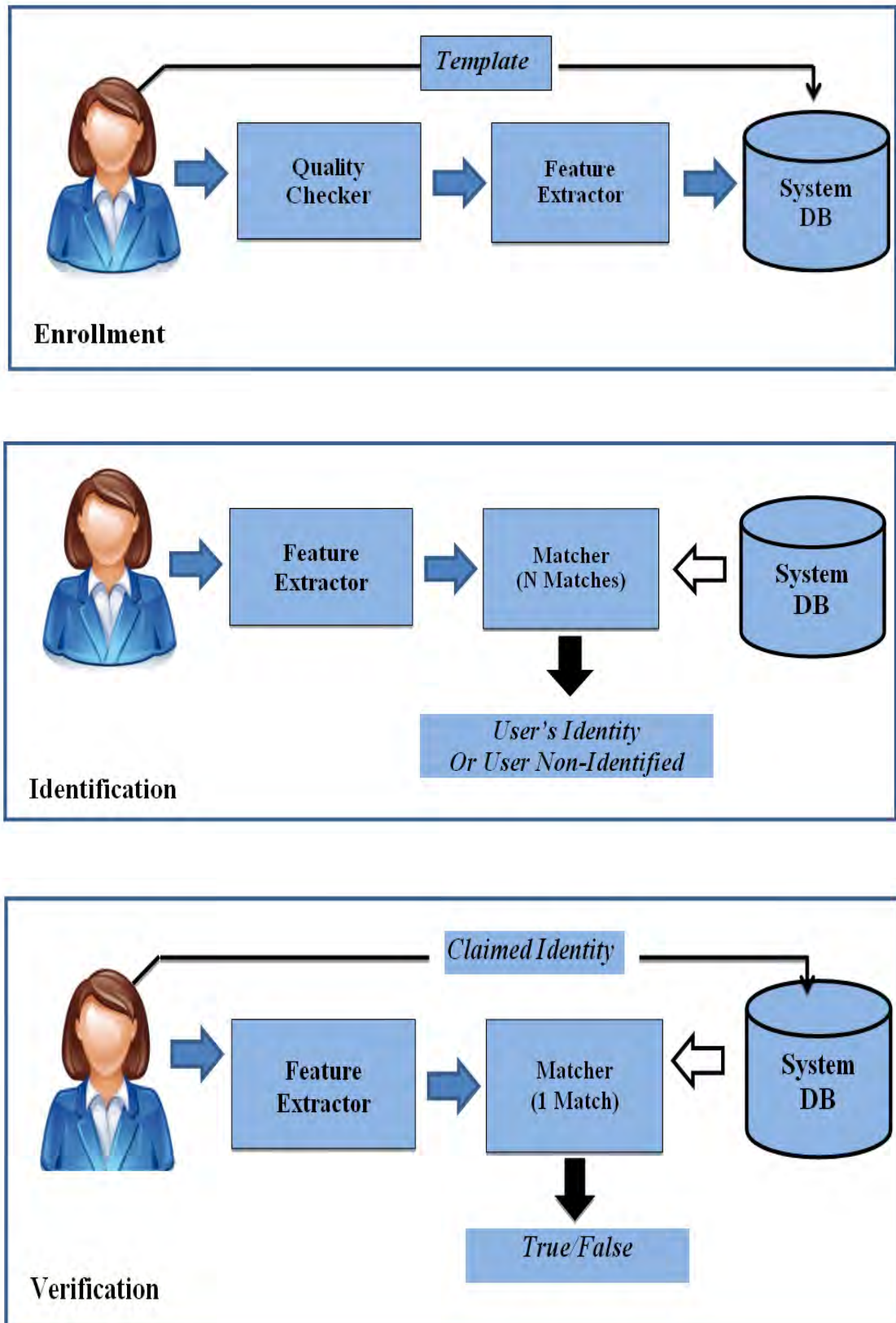


Fig. 2.1: Block diagrams of enrollment, verification, and identification tasks are shown using the four main modules of a biometric system, i.e., sensor, feature extraction, matcher, and system database.

The verification problem may be formally posed as follows: given an input feature vector X_Q (extracted from the biometric data) and a claimed identity I , determine if (I, X_Q) belongs to class w_1 or w_2 , where w_1 indicates that the claim is true (a genuine user) and w_2 indicates that the claim is false (an impostor). Typically, X_Q is matched against X_I , the biometric template corresponding to a user I , to determine its category. Thus,

$$(I, X_Q) \in \begin{cases} w_1, & \text{if } S(X_Q, X_I) \geq t \\ w_2, & \text{otherwise} \end{cases} \quad (2.1)$$

where S is the function that measures the similarity between feature vectors X_Q and X_I , and t is a predefined threshold. The value $S(X_Q, X_I)$ is termed as a similarity or matching score between the biometric measurements of the user and the claimed identity. Therefore, every claimed identity is classified into w_1 or w_2 based on the variables X_Q , I , X_I , and t , and the function S . Note that biometric measurements (e.g., fingerprints) of the same individual taken at different times are almost never identical. This is the reason for introducing the threshold t .

The identification problem, on the other hand, may be stated as follows: given an input feature vector X_Q , determine the identity I_k , $k \in [1, N, N+1, N, N+1]$. Here I_1, I_2, \dots, I_N are the identities enrolled in the system, and I_{N+1} indicates the rejected case where no suitable identity can be determined for the user. Hence,

$$X_Q \in \begin{cases} I_k, & \text{if } \max\{S(X_Q, X_{I_k})\} \geq t, k = 1, 2, \dots, N \\ I_{N+1}, & \text{otherwise} \end{cases} \quad (2.2)$$

Where X_{I_k} is the biometric template corresponding to identity I_k , and t is a predefined threshold.

2.1.2.3 Modules in Biometric System

A biometric system is built with the four major elements listed below:

- a) **Sensor module:** It collects an individual's biometric data. A fingerprint sensor that photographs the ridge and valley structure of a user's finger is one example.

- b) **Feature extraction module:** This module processes the obtained biometric data to extract a collection of prominent or discriminating characteristics. In the feature extraction module of a fingerprint-based biometric system, for example, the location and orientation of minutiae points (local ridge and valley singularities) in a fingerprint picture are retrieved.
- c) **Matcher Module:** In this module, the characteristics recognized during recognition are compared to the stored templates to generate matching scores. For example, the matching module of a fingerprint-based biometric system determines the number of matching minutiae between the input and template fingerprint pictures and reports a matching score. The matcher module also includes a decision-making module, which uses the matching score to affirm or establish a user's stated identity (verification).
- d) **System Database Module:** The biometric system uses the system database module to store the biometric templates of the enrolled users. The enrollment module is in charge of enrolling people in the biometric system database. During the enrollment step, an individual's biometric characteristic is initially scanned by a biometric reader to generate a digital representation (feature values) of the characteristic. Depending on the program, data gathering throughout the enrollment process may or may not be overseen by a human. A quality check is usually done to guarantee that the obtained sample can be processed reliably by subsequent steps. For easier matching, the digital input representation is further processed by a feature extractor to create a compact yet expressive representation known as a template. Depending on the application, the template may be kept in the biometric system's central database or on a smart card provided to the individual. To account for changes in the biometric characteristic, several templates of an individual are typically kept, and the templates in the database may be changed over time.

2.1.3 Biometric Devices

Several biometric characteristics exist and are in use in various applications. Each biometric has its strengths and weaknesses, and the choice depends on the application. No single biometric is expected to effectively meet the requirements of all the

applications. In other words, no biometric is “optimal.” The match between a specific biometric and an application is determined depending upon the operational mode of the application and the properties of the biometric characteristic.

Various Biometric Technologies that were designed till now are as given below:

- ❖ DNA Fingerprinting
- ❖ Vein Thermogram
- ❖ Face Recognition
- ❖ Fingerprint
- ❖ Hand and Finger Geometry Recognition
- ❖ Iris Scanning
- ❖ Retina Scanning
- ❖ Signature Verification
- ❖ Voice Recognition
- ❖ Ear Scanning
- ❖ Gait Sequence Analyzing
- ❖ Keystroke Analyzing
- ❖ Odor Sensing
- ❖ Palmprint Recognition

Of these, the last five viz: Ear Scanning, Gait Sequence Analyzing, Keystroke Analyzing, Odor Sensing, and Palmprint Recognition are not very effective.

2.2 Iris Structure

The iris is the colourful part of the eye that controls the quantity of light that enters the pupil. It consists of those different layers: the stroma or pigmented outer tissue. It consists of the iris sphincter muscle and iris dilatory muscle that contract and spread the iris. It consists of the anterior pigment myopithel, which is related to the muscular procedures of the iris dilator muscle. Furthermore, the iris is separated into two zones,

comprising the pupil area and the ciliary area. These two areas are separated by a single cell line, a collarette. The iris colouring varies between people and is hazel, grey, blue, green, and brown.

The iris, like the ciliary body, is a continuation of the retina and choroid. It is attached to the ciliary body and extends in front of the lens.

2.2.1 Iris Features

The iris begins to form in the third month of gestation [26] and the structures creating its pattern are largely complete by the eighth month, although pigment accretion can continue into the postnatal years. Its complex pattern can contain many distinctive features such as arching ligaments, furrows, ridges, crypts, rings, corona, freckles, and a zigzag collarette. Iris colour is determined mainly by the density of melanin pigment [27] in its anterior layer and stroma, with blue irises resulting from an absence of pigment: long-wavelength light penetrates and is absorbed by the pigment epithelium, while shorter wavelengths are reflected and scattered by the stroma.

2.2.1.1 The Crypts and Furrows

The Crypts of Fuchs are a series of openings located on either side of the collarette that allows the stroma and deeper iris tissues to be bathed in aqueous humour. Collagen trabeculae that surround the border of the crypts can be seen in blue irides.

The pupillary ruffs (crenations) are a series of small ridges at the pupillary margin formed by the continuation of the pigmented epithelium from the posterior surface.

The Circular contraction folds, also known as contraction furrows, are a series of circular bands or folds about midway between the collarette and the origin of the iris. These folds result from changes in the surface of the iris as it dilates.

Crypts at the base of the iris are additional openings that can be observed close to the outermost part of the ciliary portion of the iris. This one is not strictly related to pupil dilation, but it's too good to leave out.

2.2.1.2 Freckles

Eye freckles are areas of the eye where the overlaying "skin" is thin enough that it becomes transparent. The freckles or spots that are visible are usually gray and are actually inside the eyeball.

Another name for eye freckles is a choroidal nevus. It is a more advanced term that doctors usually use. Eye freckle is the easier name among normal people. There are various reasons why an eye freckle may develop inside the eye. Some people are born having this freckle inside their eyes. Some others develop it during childhood or even when they are adults. Too much exposure to sunlight can be one of the reasons. So make sure you keep your eyes protected by wearing sunglasses when in strong sunlight. Although eye freckles are not necessarily a "normal" finding in our eyes, they are quite common and may not represent anything wrong with the eye.

2.2.1.3 ZigZag Collarette

The iris complex pattern's zigzag collarette section is one of the essential components of the pattern. It is insensitive to pupil dilation and is not impacted by the eyelid or eyelash unless the pupil is partially obscured by the eyelid or eyelash, in which case it is affected by the pupil dilation. Certain studies have revealed that zigzag collarette areas are usually concentric with the pupil and that the radius of zigzag collarette areas is constrained to a specific range of values. The zigzag collarette area can be easily identified by looking through the center of the pupils. Some samples are shown in Fig. 2.2.

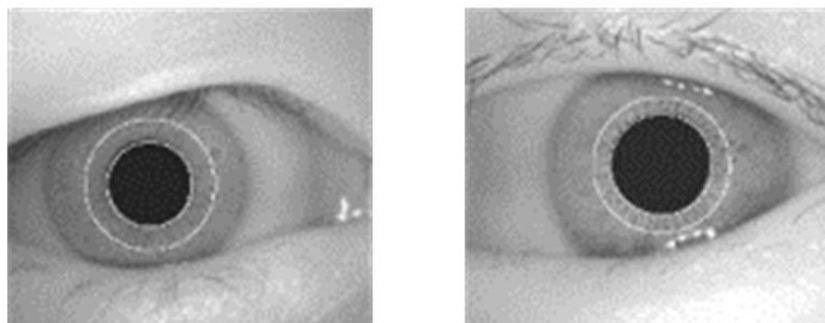


Fig. 2.2: Zigzag Collarette area localization from CASIA iris database

2.3 Iris Recognition System Errors

False accept (FA): Accepting an imposter as an authorized subject.

False reject (FR): Rejecting an authorized subject incorrectly.

Equal error (EE): When FA and FR are equal, the error is referred to as equal error.

FAR: FAR is the measure of the likelihood that the biometric security system would incorrectly accept an attempt by an unauthorized user (Imposter). Fig. 2.3 depicts the process of FAR.

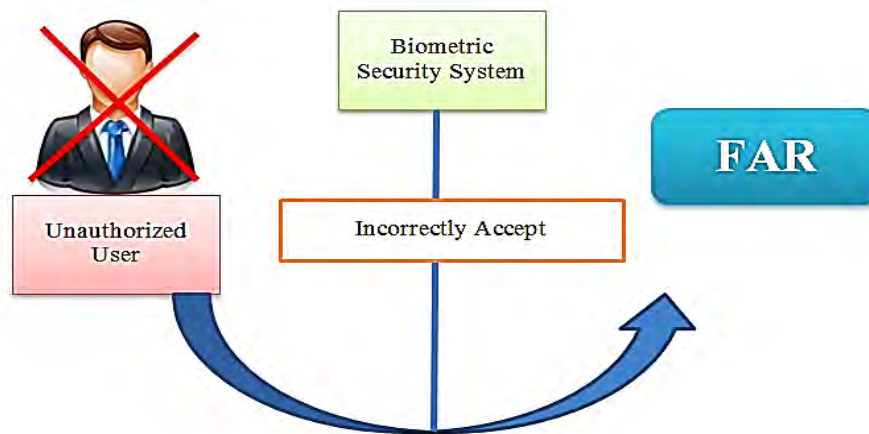


Fig. 2.3: Illustration of FAR

FRR: FRR is the measure of the likelihood that the biometric security system would incorrectly reject an attempt by an authorized user (Genuine). Fig. 2.4 depicts the process of FAR.

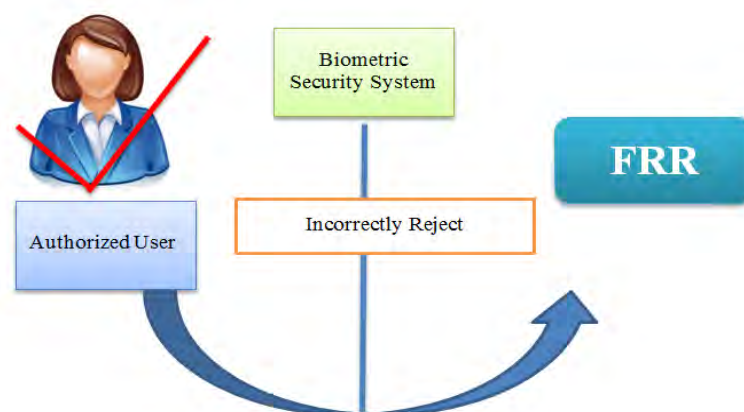


Fig. 2.4: Illustration of FRR

2.4 Comparison of Iris Recognition with Other Biometrics

Some relative comparisons of biometric security systems are listed below. The main advantages of an iris recognition system over other biometric systems are the highest accuracy, reliability, non-invasive, highest speed, etc.

Table 2.1: Comparison of different biometric security systems

Comparison title	Iris recognition	Finger prints	Facial recognition	Hand geometry
Accuracy	Highest accuracy: It had no false matches in over 2 million cross-comparisons.	The fingerprint is not as accurate. Its FAR is 1 in 100,000.	Lighting, age, glasses, and head/face coverings all impact false reject rates.	Weather, temperature and medical condition can affect hand size and accuracy.
Privacy	Convenient: Image is non-invasive and inherently safe.	N/A	Image can be used without explicit opt-in permission	N/A
Equipment	Extremely low maintenance costs.	Wide range of vendors and solutions.	Easy to deploy, can use standard CCTV	Fairly expensive equipment is required.
Physical characteristics	240 characteristics to create the unique Iris Code.	Approximately 40-60 characteristics.	N/A	N/A
Uniqueness	Iris pattern has vastly more randomness.	It has less uniqueness compared to the iris pattern.	Face structures have some uniqueness, but it's not overwhelming.	N/A
Stable	The iris itself is stable throughout a person's life.	User fingerprints may be obscured, damaged or changed.	Age, facial hair, surgery, head coverings, and masks all affect results.	Hand size and geometry change over time.
Hygienic issue	It does not require a hygienic issue	Users need physical contact with a scanner device that needs to be kept clean (hygiene issue).	It does not require a hygienic issue	The user needs physical contact. So there is a question about hygienic.
Speed and high volume	Ability to handle very large populations at high speed	In large-scale deployments, it takes many minutes, not seconds		Unsuitable for the high volume, large population applications

2.5 Strengths and Weakness of Iris Recognition

A progressive biometric iris is more accurate than fingerprints or faces. The iris is unique and stable over time. It is the most stable biometric on the human body. Although its superior accuracy, iris recognition has not been widely used because the technology is several time-consuming, requiring the user to stop them close to the camera and remain there for several moments. As any technology with its limitations, the iris has faced many challenges in terms of user acceptance, they think it involves a laser, and it will hurt their eye. It is also challenging because it is rather a small target about a centimeter in diameter. Some strengths and weak points of iris recognition systems are given below.

2.5.1 Strengths of Iris Recognition

- The iris patterns have small intra-class variability [5, 28].
- The iris is a well-protected internal organ of the eye that contains a high degree of randomness [28]
- The iris is externally visible, which makes iris image acquisition possible from a distance [14, 19].
- The iris pattern remains stable throughout the lifetime of a person, and it is assumed that each individual has a unique iris pattern [5].
- It is possible to encode the iris pattern, and the recognition system's decidability is tractable [29].
- No evidence of genetic influence has been found in the structure of the iris [12]. Therefore, the iris structures in both eyes of the same person are different, and those of identical twins are also different [30].
- Iris recognition systems require very low maintenance costs with high interoperability between different hardware vendors.
- Proven highest accuracy: iris recognition had no false matches in over two million cross-comparisons, according to Biometric Product Testing Final Report (19 March 2001, Center for Mathematics and Scientific Computing, National Physics Laboratory, U.K.) (Refer Table 2.2)
- Ability to handle very large populations at high speed
- Search speed: 1 million Iris Codes per second, with a 3 GHz CPU

Table 2.2: Cross-comparisons of different Biometric Products

Testing organization	Number of cross-comparisons	False matches
Sandia Labs, USA (1996)	19,701	0
British Telecom Labs, UK (1997)	222,743	0
Sensar Crop, USA (2000)	499,500	0
Joh. Enschede, NL (2000)	19,900	0
EyeTicket, USA (2001)	300,000	0
National Physical Lab, UK (2001)	2.73 million	0
J. Daugman, UK (2003)	9.1 million	0
Iridian Technologies, USA (2003)	984 million	0
<i>Source: http://www.cl.cam.ac.uk/users/jgd1000/iristests.pdf</i>		

Table 2.3: Template size of different biometrics

Biometrics	Approx. Template size
Voice	70k ~ 80k
Face	84 bytes ~ 2k
Signature	500 bytes ~ 1000 bytes
Fingerprint	256 bytes ~ 1.2 k
Hand Geometry	9 bytes
Iris	256 bytes ~ 512 bytes
Retina	96 bytes

2.5.2 Weakness of Iris Recognition

- It is difficult to capture the iris image since the size of the iris is very small (its approximate diameter is 1 cm). A specialized camera with an extensive apparatus setup is needed to acquire iris images [4, 28].
- The iris could be partially occluded by lower and upper eyelids and obscured by eyelashes, reflections, and lenses [8, 12-15, 31].
- The size of the pupil changes, non-elastic deformation is a major drawback [3, 5, 14, 28, 32].

2.6 Application of Iris Recognition

Some Current and Future Applications of Iris Recognition:

- national border controls: the iris as a living passport
- computer login: the iris as a living password

- cell phone and other wireless-device-based authentication
- secure access to bank accounts at cash machines
- ticketless travel; authentication of rights to services
- premises access control (home, office, laboratory, etc.)
- driving licenses; other personal certificates
- entitlements and benefits authorization
- forensics; birth certificates; tracing missing or wanted persons
- credit-card authentication
- automobile ignition and unlocking; anti-theft devices
- anti-terrorism (e.g., security screening at airports)
- secure financial transactions (electronic commerce, banking)
- Internet security; control of access to privileged information
- "Biometric-Key Cryptography" (stable keys from unstable templates)
- any existing use of keys, cards, PINs, or passwords

Some Currently available iris recognition services as a product:

- ❖ L1 Identity Solutions (owner and worldwide licensor of the algorithms)
- ❖ LG-Iris (largest number of deployments: more than 1,000)
- ❖ Panasonic (residential and logical access control; airport uses)
- ❖ Oki Electric Industries (access control; iris patterns in lieu of passports)
- ❖ IBM (border-crossing applications)
- ❖ Iris Guard UAE deployment, using scalable server architecture for large-scale Iris Code database searches: the Iris Farm.
- ❖ Securimetrics (portable handheld cameras for military and police use, and high-speed SIRIS search engine)
- ❖ Sagem (national biometric identification projects)
- ❖ Argus Australia (access control; pharmaceutical dispensing)
- ❖ 10 UK airport terminals (entry into the UK by iris pattern, instead of a passport)
- ❖ Amsterdam Schiphol Airport (instead of passport presentation)

2.7 Summary

The authentication of people using iris-based recognition is a widely developing technology. Iris recognition is feasible for use in differentiating between identical twins. Though the iris colour and the overall statistical quality of the iris texture may depend on genetic factors, the textural details are independent and uncorrelated for genetically identical iris pairs. As a result, iris recognition is considered one of the most reliable biometric systems. Iris-based recognition is a beneficial biometric solution to human identification due in part to the minimally intrusive nature of its data collection and the accuracy and security derived from the uniqueness of human irises.

CHAPTER 3

Iris Segmentation and Normalization

3.1 Overview

To do iris recognition, the first step is to extract the actual iris region in a digital image of the eye. Two circles can be used to approximate the iris region: one for the iris/sclera boundary and another, which is internal to the first, for the iris/pupil boundary. The upper and lower regions of the iris region are generally concealed by the upper and lower eyelids and eyelashes. Additionally, specular reflections can occur within the iris region, causing the iris pattern to become distorted. It is necessary to employ a strategy to isolate and exclude these artifacts, as well as to locate the circular iris region. The success of segmentation is dependent on the quality of the eye pictures used in the segmentation process. Due to the use of near-infrared light for illumination, the images in the CASIA iris database [13] do not contain specular reflections, as do images in other databases. In addition, individuals with darkly pigmented irises will have relatively low contrast between the pupil and iris region if their eyes are imaged under natural light, which makes the segmentation more difficult. As previously stated, segmentation is crucial to the success of an iris recognition system since data that is incorrectly represented as iris pattern data will contaminate the biometric templates generated, resulting in low recognition rates.

It is necessary to modify the iris region so that it has fixed dimensions in order to make comparisons possible after it has been successfully segmented from an eye image. It is mostly owing to pupil dilatation produced by variable levels of illumination that the differences in dimensional consistency between eye pictures can be explained by stretching of the iris. Aside from variable imaging distance, rotation of the camera and head tilt, and movement of the eye within the eye socket, other sources of inconsistency include: The normalizing method will result in iris areas that have the same constant dimensions, resulting in two images of the same iris taken under different conditions having typical features at the same spatial location in both photographs.

3.2 Image Acquisition

The first step of iris recognition is the acquisition of iris images using a special iris camera. The module of iris image acquisition defines the inter-face between the user and the iris recognition system, so its usability is critical to user experiences. Moreover, the capability of iris image acquisition determines the quality of iris images used for iris pattern recognition (refer to Fig. 3.1). Therefore, iris image acquisition is an extremely important step in an iris recognition system. However, iris image acquisition is a very challenging problem due to the following reasons:

- The iris is a very small internal organ with a diameter of about 1cm, but the resolution of the iris images must be higher enough for them to be useful for recognition, typically no less than 150 pixels across the diameter. So the depth of field (DoF) of an iris acquisition system is often limited.
- The microstructures or texture of the irises of many people, especially those of Asians, only become visible under near-infrared (NIR) lighting. So the configuration of NIR lighting is a major issue in iris image acquisition.
- When people wear eyeglasses, it is challenging to capture clear iris images due to specular reflections and dirt on eyeglasses.
- The human subject may be in motion when the iris image is being taken, so the image may be blurred due to motion.

There are several techniques for image acquisition, especially for iris biometric systems. Most biometric device Manufacturer Company develops their own camera for the acquisition of images in a proper way. Sarnoff Company proposed their iris image acquisition technique in the 1990s [3]. R.P Wilds focused on several parameters while taking the iris image for person authentication [48]. The image should acquire sharp, high resolution and also be imaged at about 128 pixels across the diameter. Regarding the person height, these images must be well centered with good contrast. Finally, the artifacts, i.e., spectacular reflection, should be eliminated from the acquired images.

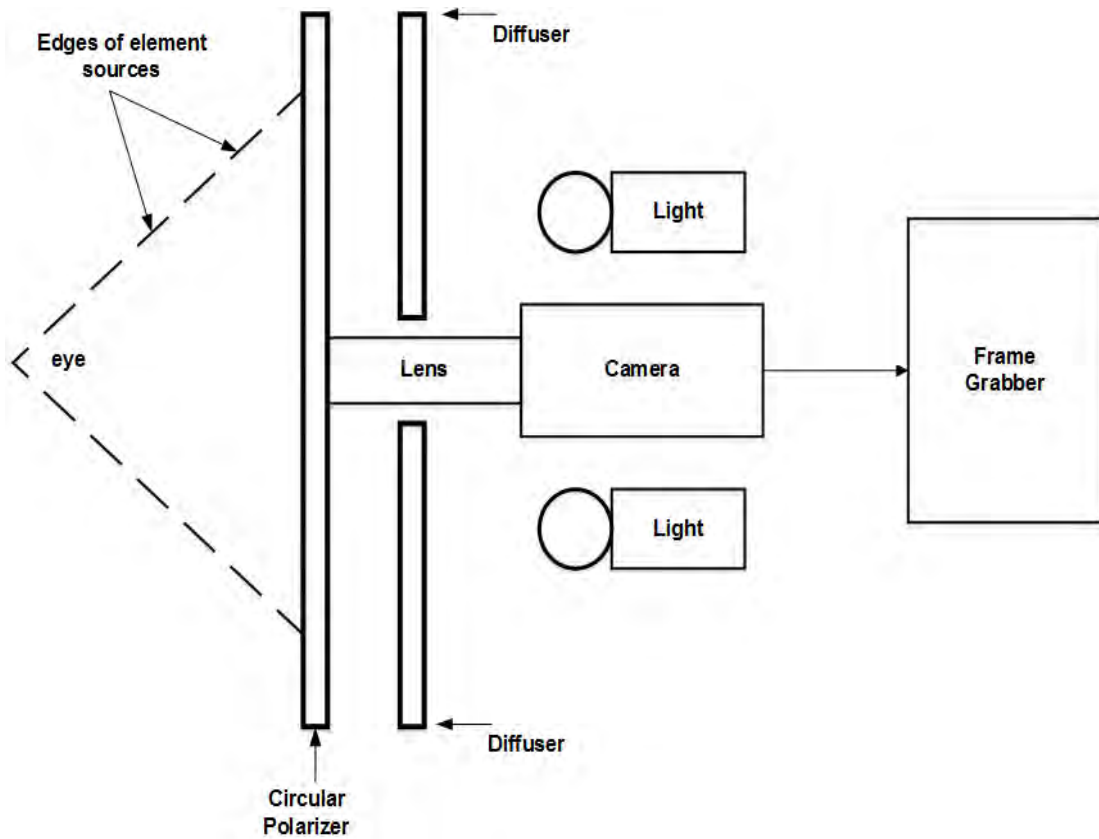


Fig. 3.1: Schematic diagram of image acquisition components

3.3 Literature Review

3.3.1 Hough Transform

The Hough transform is a standard computer vision algorithm that can be used to determine the parameters of simple geometric objects, such as lines and circles, present in an image. The circular Hough transform can be employed to deduce the radius and center coordinates of the pupil and iris regions. An automatic segmentation algorithm based on the circular Hough transform is employed by Wildes et al. [48], Kong and Zhang [55], Tisse et al. [56], and Ma et al. [7]. Firstly, an edge map is generated by calculating the first derivatives of intensity values in an eye image and then thresholding the result. From the edge map, votes are cast in Hough space for the parameters of circles passing through each edge point. These parameters are the center coordinates x_c and y_c , and the radius r , which can define any circle according to the equation,

$$x_c^2 + y_c^2 = r^2 \quad (3.1)$$

A maximum point in the Hough space will correspond to the radius and center coordinates of the circle best defined by the edge points. Wildes et al. and Kong and Zhang also make use of the parabolic Hough transform to detect the eyelids, approximating the upper and lower eyelids with parabolic arcs, which are represented as;

$$\begin{aligned} &(-(x - h_j) \sin \theta_j + (y - k_j) \cos \theta_j)^2 \\ &= a_j((x - h_j) \cos \theta_j + (y - k_j) \sin \theta_j) \end{aligned} \quad (3.2)$$

Where a_j controls the curvature, (h_j, k_j) is the peak of the parabola and θ_j is the angle of rotation relative to the x-axis.

In performing the preceding edge detection step, Wildes et al. bias the derivatives in the horizontal direction for detecting the eyelids and in the vertical direction for detecting the outer circular boundary of the iris; this is illustrated in Fig. 3.2. The motivation for this is that the eyelids are usually horizontally aligned, and also the eyelid edge map will corrupt the circular iris boundary edge map if using all gradient data. Taking only the vertical gradients for locating the iris boundary will reduce the influence of the eyelids when performing circular Hough transform, and not all of the edge pixels defining the circle are required for successful localization. Not only does this make circle localization more accurate, but it also makes it more efficient since there are fewer edge points to cast votes in the Hough space.

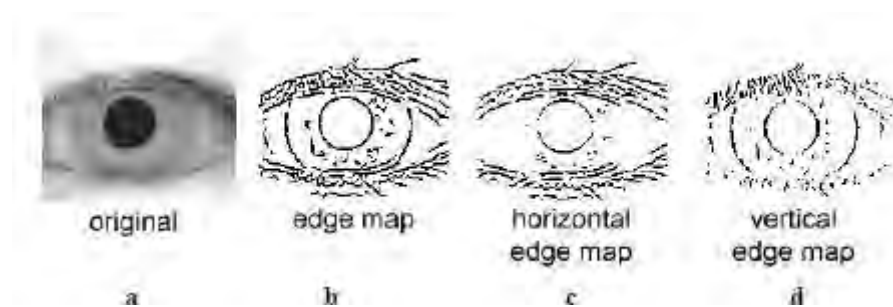


Fig. 3.2: (a) an eye image (020_2_1 from the CASIA database) (b) corresponding edge map (c) edge map with only horizontal gradients (d) edge map with only vertical gradients.

There are a number of problems with the Hough transform method. First of all, it requires threshold values to be chosen for edge detection, and this may result in critical edge points being removed, failing to detect circles/arcs. Secondly, the Hough

transform is computationally intensive due to its ‘brute-force’ approach and thus may not be suitable for real-time applications.

Iris boundary localization algorithm is as follows:

- ❖ **Step 1.** Pupil center coarse localization;
- ❖ **Step 2.** Select a small image block and extract edge information based on the canny operator;
- ❖ **Step 3.** Pupil boundary localization based on Hough transform;
- ❖ **Step 4.** Select a small image block and extract edge information based on the line’s grey gradient extreme value;
- ❖ **Step 5.** Iris outer boundary localization based on Hough transforms. Due to improve localization speed and localization accuracy, taking advantage of the grey information, the number of edge points has to be decreased and the parameter range down to a small range to locate iris boundary.

3.3.2 Daugman’s Integro-differential Operator

Daugman’s integrodifferential equation can be applied to find the center coordinates as well as the radius of the iris and the pupil. This equation can be stated as follows [11]

$$\max_{(r,x_0,y_0)} \left| G_\sigma(r) * \frac{\partial}{\partial r} \oint_{r,x_0,y_0} \frac{f(x,y)}{2\pi r} ds \right| \quad (3.3)$$

Where $I(x,y)$ is an image containing an eye. The operator searches over the image domain (x,y) for the maximum in the blurred partial derivative with respect to increasing radius r of the normalized contour integral of $I(x,y)$ along with a circular arc ds of radius r and center coordinates (x_0,y_0) . The symbol $*$ denotes convolution, and $G_\sigma(r)$ is a smoothing function such as a Gaussian of scale σ . The complete operator behaves in effect as a circular edge detector, blurred at a scale set by σ , which searches iteratively for a maximum contour integral derivative with increasing radius at successively finer scales of analysis through the three-parameter space of center coordinates and radius (x_0,y_0,r) defining a path of contour integration. The

operator searches for the circular path where there is the maximum change in pixel values by varying the radius 'r' and the center (x, y) of the circular contour. The operator is applied iteratively with the amount of smoothing progressively reduced in order to obtain accurate localization.

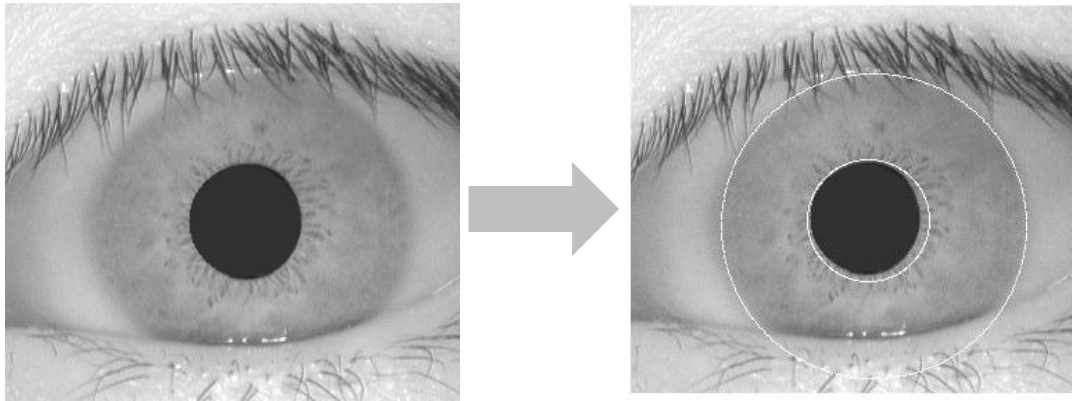


Fig. 3.3: Assuming r_{min} , r_{max} : (90, 110) the minimum and maximum values of the iris radius using Daugman's integrodifferential operator.

Function to search for the centre coordinates of the pupil and the iris along with their radii. It makes use of Camus&Wildes' method to select the possible centre coordinates first. The method consists of thresholding followed by checking if the selected points (by thresholding) correspond to a local minimum in their immediate (3*s) neighbourhood. These points serve as the possible centre coordinates for the iris. Once the iris has been detected (using Daugman's method); the pupil's centre coordinates are found by searching a 10*10 neighbourhood around the iris centre and varying the radius until a maximum is found (using Daugman's integrodifferential operator).

Assuming that the variables x , y and r belong to the ranges $[0; X]$, $[0; Y]$ $[0; R]$ respectively, this method has the computational complexity of order $[X \times Y \times R]$. Thus, at every pixel, a total of R scans are necessary to compute the circle parameters using this approach.

3.3.2 Eyelash and Noise Reduction

Kong and Zhang [15] present a method for eyelash detection, where eyelashes are treated as belonging to two types, separable eyelashes, which are isolated in the

image, and multiple eyelashes, which are bunched together and overlap in the eye image. Separable eyelashes are detected using 1D Gabor filters since the convolution of a separable eyelash with the Gaussian smoothing function results in a low output value. Thus, if a resultant point is smaller than a threshold, it is noted that this point belongs to an eyelash. Multiple eyelashes are detected using the variance of intensity. If the variance of intensity values in a small window is lower than a threshold, the center of the window is considered as a point in an eyelash (refer to Fig. 3.4). The Kong and Zhang model also makes use of connective criteria so that each point in an eyelash should connect to another point in an eyelash or to an eyelid. Specular reflections along the eye image are detected using thresholding since the intensity values at these regions will be higher than at any other region in the image.

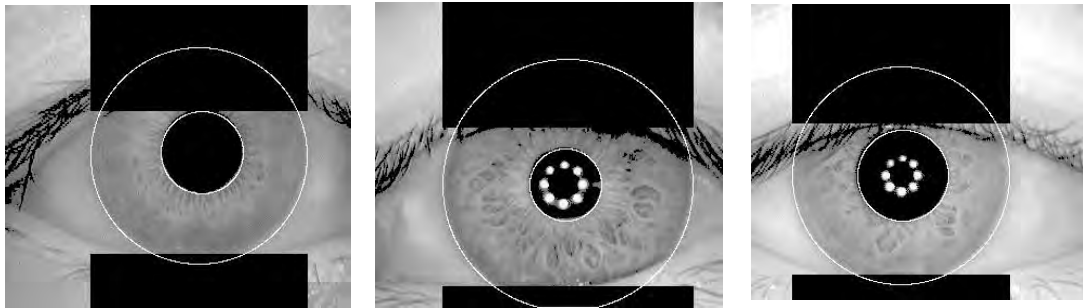


Fig. 3.4: The eyelash detection technique, eyelash regions are detected using thresholding and denoted as black

3.4 Morphology and Geometrical Approach Iris Localization

A two-stage iris segmentation algorithm has been applied in this stage. Firstly, a manual edge point evolution approach based on binary morphology has been applied to detect the inner boundary. In the second stage, the geometrical operation via the image intensity has been utilized in order to find the iris center and, finally, the iris boundary. Iris Inner and Outer boundary localization algorithm can be described as follows.

3.4.1 Inner and Outer Boundary Localization

Iris Inner and Outer boundary localization algorithm can be described as follows:

- ❖ **Step 0.** The original Eye image captured by an imaging sensor
- ❖ **Step 1.** Obtained the binary image of the iris;

- ❖ **Step 2.** Obtained the Medfilt image of the binary image.
- ❖ **Step 3.** Image Compliment
- ❖ **Step 4.** Removing Small areas
- ❖ **Step 5.** Finding pupil center with pupil boundary.
- ❖ **Step 6.** Apply appropriate threshold

$$\cos \theta = (X - X_0)/R \quad (3.4)$$

$$\cos\left(\frac{\pi}{2} - \theta\right) = (Y - Y_0)/R \quad (3.5)$$

- ❖ **Step 7.** Adjusted the image and studied the image intensity
- ❖ **Step 8.** Determine the iris boundary
- ❖ **Step 9.** Connect the two points of iris boundary
- ❖ **Step 10.** Finding the center of lines.
- ❖ **Step 11.** Apply two horizontal lines. The theory behind this, i.e., The horizontal line from the middle of the radius in any circle passes through the center of the circle
- ❖ **Step 12.** The intersection of two horizontal lines is the required iris center. This can be found by this equation:

$$\frac{r_2 - r_1}{c_2 - c_1} = \frac{R - r_2}{C - c_2} \quad (3.6)$$

$$\frac{r_4 - r_3}{c_4 - c_3} = \frac{R - r_4}{C - c_4} \quad (3.7)$$

- ❖ **Step 13.** Calculating the radius and area by the following equation

$$R = \sqrt{(c_1 - c_0)^2 + (r_1 - r_0)^2} \quad (3.8)$$

$$A = 2\pi R \quad (3.9)$$

- ❖ **Step 14.** Finally, the area will be detected.



Step 0



Step 1



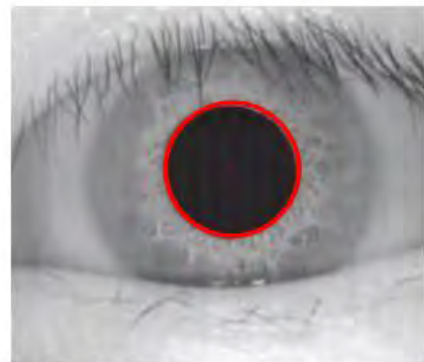
Step 2



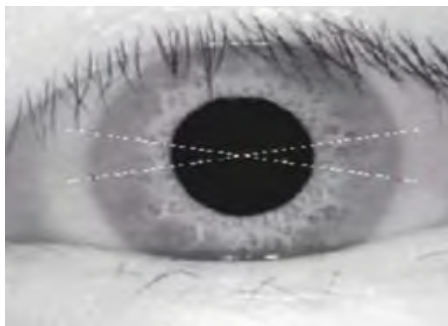
Step 3



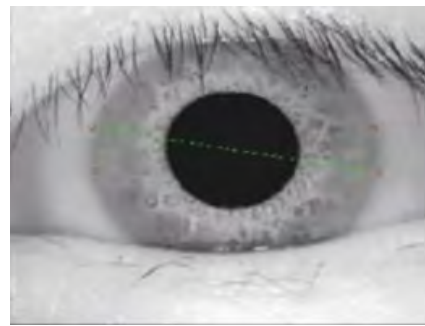
Step 4



Step 5



Step 6



Step 7

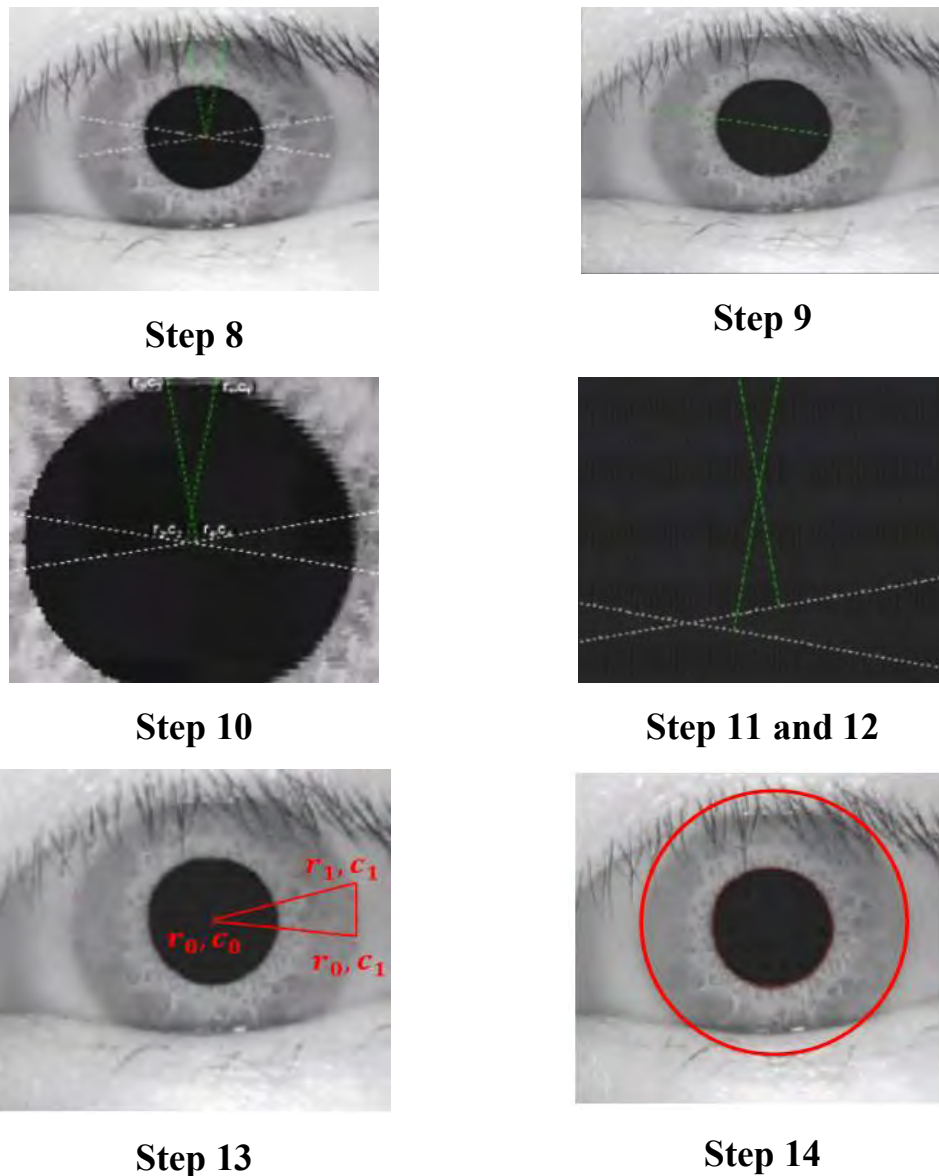


Fig. 3.5: Illustration of Iris localization steps according to the Morphology and Geometrical algorithm

Algorithms: Estimation of the center of Pupil

Input: $f(s,t)$ (the iris image), The Complement iris image

Output: $o(s_c, t_c)$ (the pupillary center) and the R_{Max} (Pupillary Radius)

1. To find the Brightest point (s_{p1}, t_{p2}) on the upper side of the pupil
2. $p_1 \leftarrow store(f(s,t))$ $q_1 \leftarrow store(f(s,t))$
3. To find the Brightest point (s_{p2}, t_{p2}) on the Bottom side of the pupil
4. $p_2 \leftarrow store(f(s,t))$ $q_2 \leftarrow store(f(s,t))$

5. To find the Brightest point (s_{s1}, t_{t1}) on the Left side of the pupil
6. $s_1 \leftarrow store(f(s, t))$ $r_1 \leftarrow store(f(s, t))$
7. To find the Brightest point (s_{s2}, t_{t2}) on the Right Side of the pupil
8. $s_2 \leftarrow store(f(s, t))$ $r_2 \leftarrow store(f(s, t))$
9. The Pupillary center $(s_c, t_c) \leftarrow (round(\frac{p1+p2}{2}), round(\frac{s1+s2}{2}))$
10. The Pupillary Radius do

$$D_1 \leftarrow store(\sqrt{(s_c - p1)^2 + (t_c - q1)^2})$$

$$D_2 \leftarrow store(\sqrt{(s_c - p2)^2 + (t_c - q2)^2})$$

$$D_3 \leftarrow store(\sqrt{(s_c - r1)^2 + (t_c - s1)^2})$$

$$D_4 \leftarrow store(\sqrt{(s_c - r2)^2 + (t_c - s2)^2})$$

11. The Pupillary Radius

$$R_{Max} \leftarrow round [Max \left(\sum_{N=4} D_N \right)]$$

12. return (s_c, t_c) and R_{Max}
-

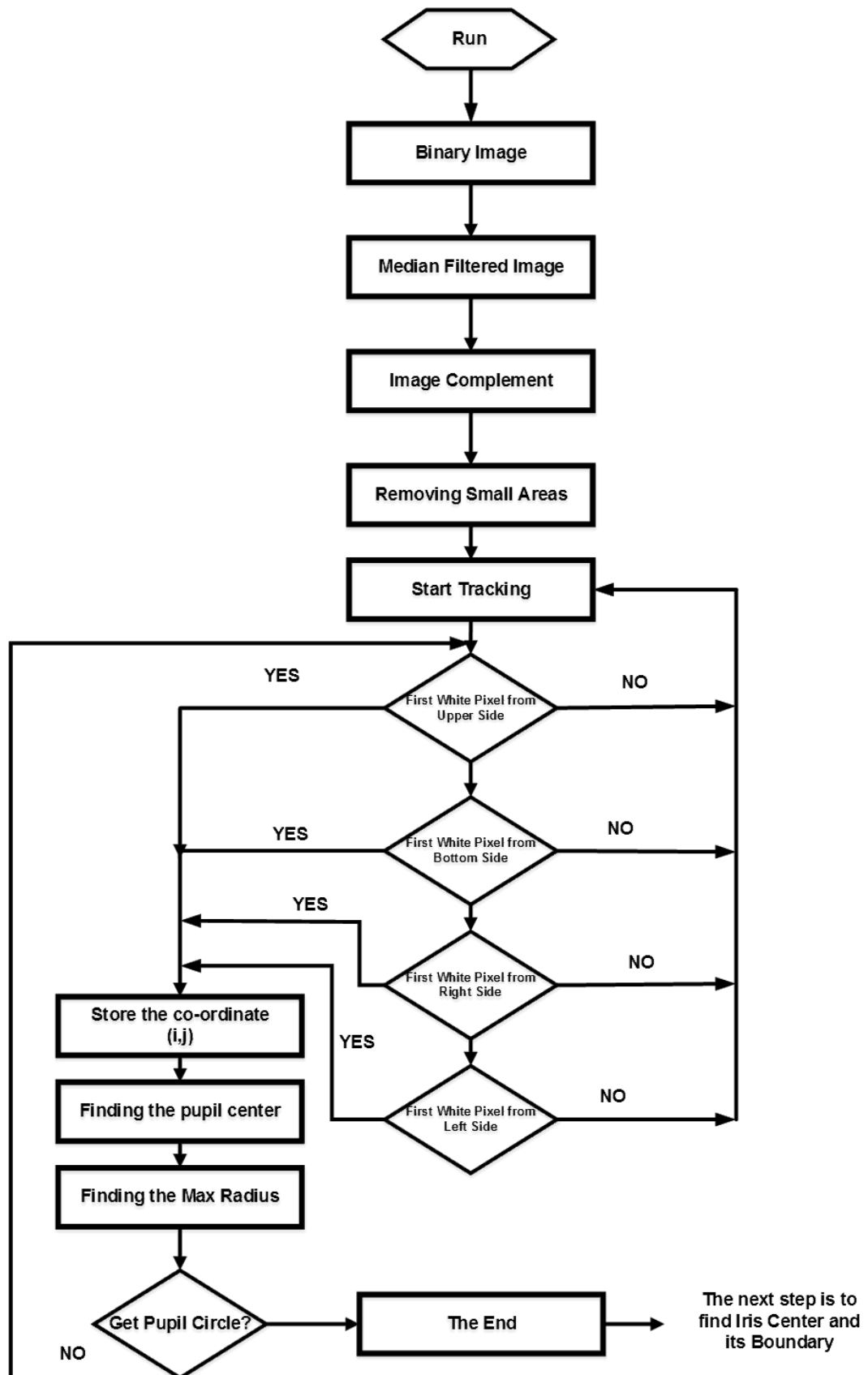


Fig. 3.6: Flow Diagram of finding Pupil Center and its Boundary/Radius

3.5 Experimental Result of Segmentation Stage

In order to evaluate the performance of the Morphology and Geometrical approach proposed in my undergraduate thesis [33], it has been applied to the CASIA ver1.0 database, and present a detailed comparison with the methods of Daugman and Wildes, implemented according to the published papers [5, 9, 34] and the open codes of MASEK [31]. All of the algorithms are implemented in MATLAB and executed on a computer (Intel Core i7-4500U CPU, 2.40 GHz, 12Gb RAM). Note that the original eye images are classified into class I (lighter interfered) and class II (seriously interfered), according to the extent to which iris boundaries are overlapped by eyelash and eyelid. All of the experiments have been completed in same environment.

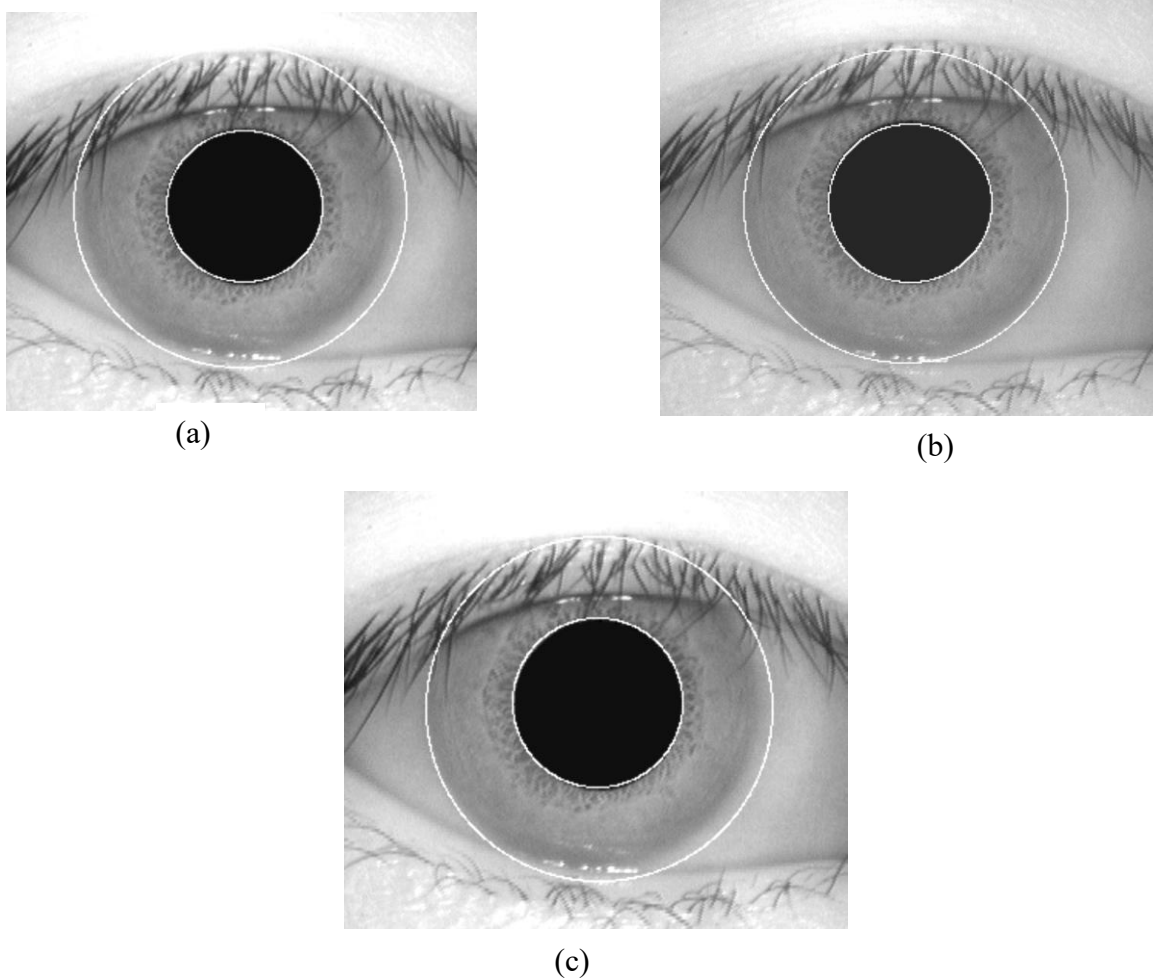


Fig. 3.7: Location results for class I: (a) Daugman's method (b), Wildes' method, (c) Morphology and Geometrical approach

This experiment is designed to compare the location performance of the three methods. Figs. 3.7 and 3.8 show the location result for class I and class II respectively. Obviously, Fig. 3.7 shows that all three methods can locate the iris boundaries correctly, and there are hardly any differences between the results. Certainly, it suggests that the proposed method can locate the iris, and the new idea of the proposed method is right. From Fig. 3.8, one can see that Daugman's and Wildes' methods give incorrect results, but the result of the Morphology and Geometrical approach is satisfactory. This experiment shows that the proposed method can complete iris location even for a seriously interfered image. It is more robust than Daugman's and Wildes' methods.

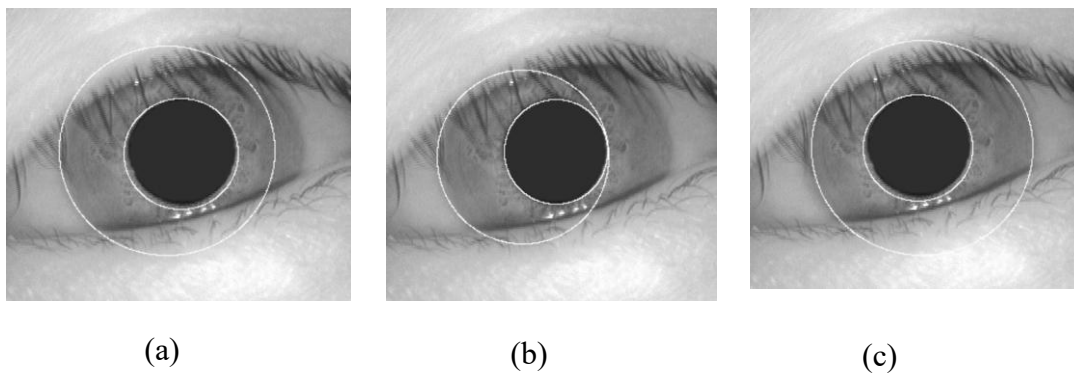


Fig. 3.8: Location results for class II: (a) Daugman's method (b) Wildes' method (c) Morphology and Geometrical approach

Table 3.1: Results obtained with the use of three methods for different classes

Method	Time [sec]		CLR [%]	
	I	II	I	II
Daugman	6.82	8.26	94.6	93.1
Wildes	11.75	12.68	94.8	92.4
Morphology and Geometrical approach [33]	2.45	3.10	97.26	98.10

Table 3.2: Results obtained with the use of three methods for all images (CLR: correct location ratio)

Method	CLR [%]	Time [sec]
Daugman	93.85	7.52
Wildes	93.6	12.24
Morphology and Geometrical approach [33]	97.85	2.45

In the experiment, a comparison was made of the correct location ratio and the expenditure of time of the three methods. Table 3.1 shows the results obtained using the three methods with reference to a particular class, and Table 3.2 lists the results for both classes. Table 3.1 is designed to test whether the Morphology and Geometrical approach can give a perfect performance or not. By quantitative data, the difference between these methods can be illustrated clearly. From Table 3.1, it follows that the proposed method has better performance than the other methods for both classes. Whether it is class I or class II, the Morphology and Geometrical approach not only reduces the location errors but makes it more computationally efficient. So, it can be concluded that the proposed method is more robust than the other methods so far as the interference of eyelashes is concerned.

3.6 Daugman's Rubber-Sheet Model

The normalization locates the outer and inner borders to reimburse the varying size and capturing distance. The size of the iris of the same eye might change because of the distance from the camera, illumination, variations, etc. The non-concentric characteristics of the iris and the pupil may affect the result of matching. According to Daugman's rubber sheet model, each pixel is mapped into a pair of polar coordinates (r, θ) where r is on the interval $[0,1]$ and θ is angle $[0,2\pi]$ as shown in Fig. 3.9.

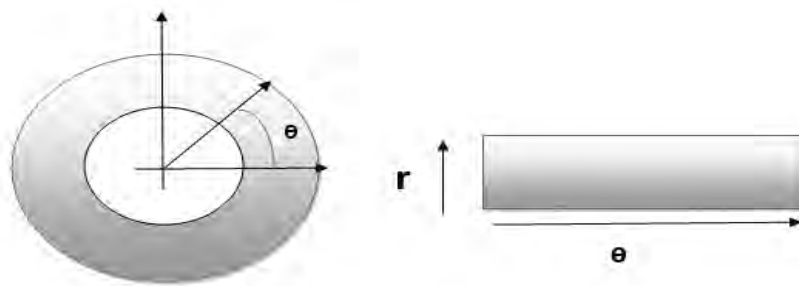


Fig. 3.9: Daugman's rubber sheet model

The unwrapping formula is as follows:

$$I(x(r, \theta), y(r, \theta)) \rightarrow I(r, \theta) \quad (3.10)$$

$$x(r, \theta) = (1 - r)x_p(\theta) + rx_i(\theta) \quad (3.11)$$

$$y(r, \theta) = (1 - r)y_p(\theta) + ry_i(\theta) \quad (3.12)$$

Where,

$$x_p(\rho, \theta) = x_{p0}(\theta) + r_p * \cos \theta \quad (3.13)$$

$$y_p(\rho, \theta) = y_{p0}(\theta) + r_p * \sin \theta \quad (3.14)$$

$$x_i(\rho, \theta) = x_{i0}(\theta) + r_i * \cos \theta \quad (3.15)$$

$$y_i(\rho, \theta) = y_{i0}(\theta) + r_i * \sin \theta \quad (3.16)$$

Where, $x(r, \theta)$ and $y(r, \theta)$ are the combinations between the coordinates of the pupillary boundaries $(x_p(\theta), y_p(\theta))$ and the coordinates of the iris boundary $(x_i(\theta), y_i(\theta))$, in the direction θ while r_p and r_i are respectively the radius of the pupil and the iris and $(x_{p0}, y_{p0}), (x_{i0}, y_{i0})$ are the centers of pupil and iris, respectively. Due to having non-concentric property of the pupil compared to the iris, a remapping formula is needed to rescale points depending on the angle round the circle given by equations:

$$r' = \sqrt{\alpha\beta} \pm \sqrt{\alpha\beta^2 - \alpha - r_i^2} \quad (3.17)$$

With, $\alpha = o_x^2 + o_y^2$, $\beta = \cos(r - \arctan(\frac{o_x}{o_y})) - \theta$

Where, r' is the distance between the edge of the pupil and edge of the iris at an angle θ around the region, the displacement of the center of the pupil relative to the center of the iris is given by o_x, o_y and r_i is the radius of the iris. Fig. 3.10 depicts the output of the normalization of the CASIA-V4-iris image with the help of the remapping formula.

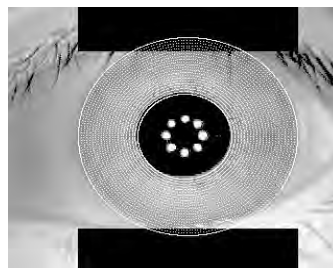


Fig. 3.10: Output of Normalization

Algorithm: Normalization

Step 1: Initialize radial resolution =18 and angular resolution =230.

Step 2: Calculate displacement of pupil center from the iris center by equation

$$r' = \sqrt{\alpha}\beta \pm \sqrt{\alpha\beta^2 - \alpha - r_i^2}$$

With, $\alpha = o_x^2 + o_y^2$, $\beta = \cos(r - \arctan\left(\frac{o_x}{o_y}\right) - \theta)$

Step 3: Exclude values at the boundary of the pupil iris border and the iris sclera border.

Step 4: Calculate the Cartesian location of each data point around the circular iris by

$$x = r \cos \theta, y = r \sin \theta$$

Step 5: Extract intensity values into the normalized polar representation through interpolation.

Step 6: Store it in a polar array. Create a noise array with the location of NaN (Not a Number) values in the polar array.

3.6.1 Implementation

Normalization generates a fixed dimension feature vector for better recognition. Daugman's rubber sheet model maps each point in the (x, y) domain to polar coordinates (r, h). The pupil center is measured as the reference point for the radial vectors to pass through the region of the iris. The radial resolution is defined as the number of data points along each radial line, and the angular resolution is defined as the number of data points going around the iris region. A fixed number of points are selected along each radial line regardless of how wide or narrow the radius is at an angle. The angular and radial positions in the normalized pattern create the Cartesian coordinates of the data points. Normalization produces a 2D array with a vertical dimension of radial resolution and a horizontal dimension of angular resolution.

Another 2D array is created for marking eyelids, eyelashes and specular reflections detected in the segmentation stage. The data points that occur along the pupil border or the iris border are discarded to prevent the non-iris region from corrupting the normalized representation. Once the eyelids and eyelashes are detected, the noisy area is mapped to be masked, and the iris without noise is extracted.



Fig.3.11: Unwrapping Normalized Iris; CASIA [S1211L04]



Fig. 3.12: Unwrapping Normalized Iris; [S1211L05]

The normalization process proved to be successful, and some results are shown in Figs. 3.11-3.12. However, the normalization process was not able to perfectly reconstruct the same pattern from images with varying amounts of pupil dilation since the deformation of the iris results in small changes in its surface pattern. The pupil is smaller in the image; however, the normalization process is able to rescale the iris region so that it has a constant dimension. In this example, the rectangular representation has a constant dimension ($M \times N$) is (64×512) .

3.6.2 Enhancement of Normalization Image

Once the iris Normalization is successfully done from the segmented iris image, the next stage is to enhance the normalized image for better feature extraction. Histogram

equalization technique has been applied for image contrast enhancement. The enhanced image is then used for the next stage, feature encoding. The corresponding histogram is shown in Fig. 3.13.

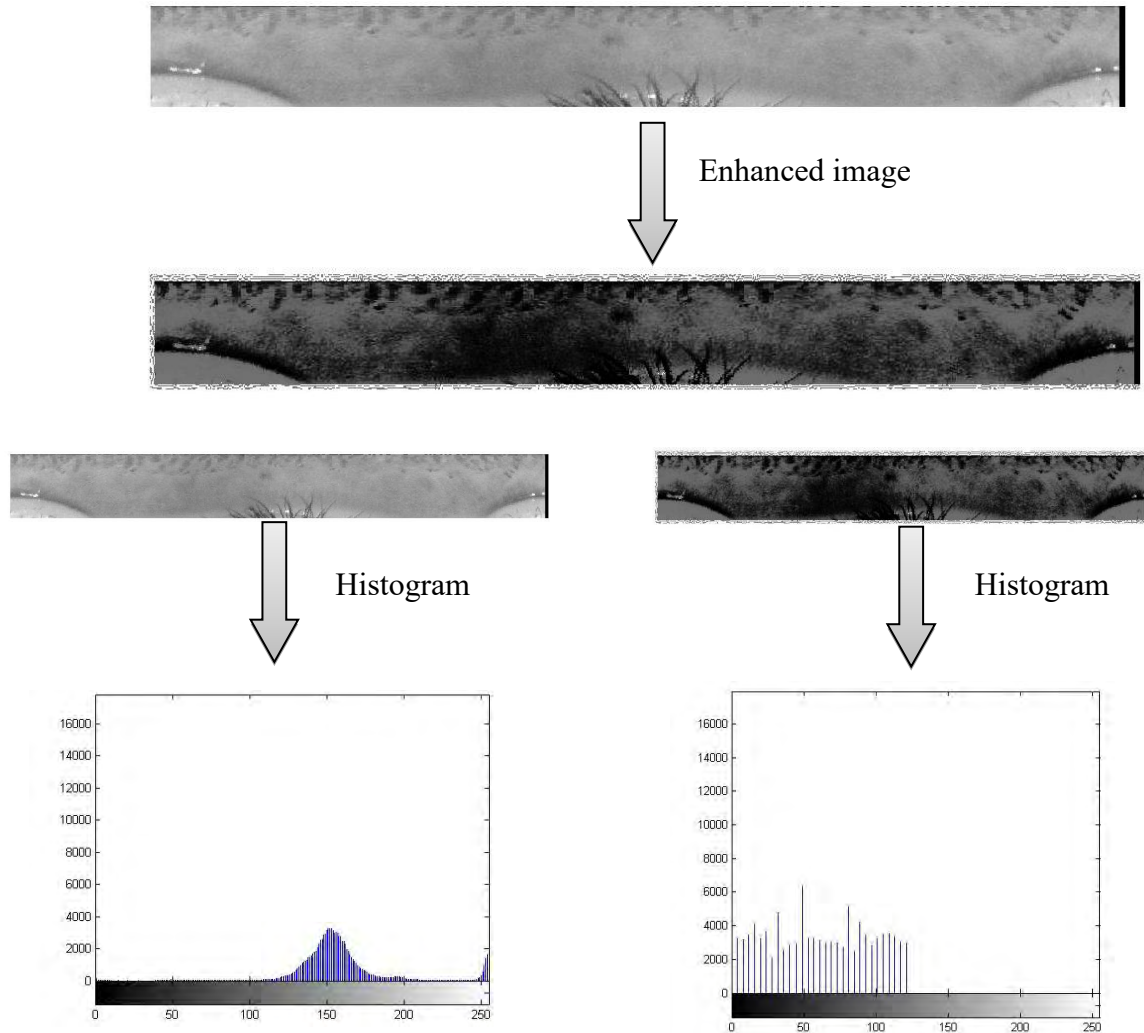


Fig. 3.13: Enhanced normalized image with the histogram

3.6 Summary

Iris segmentation is a crucial stage of the iris recognition system because the accuracy of recognition mainly depends on the accurate localization of the iris inner and outer boundary with minimally affected by eyelids and eyelashes. The proposed segmentation approach considerably reduces the computation and time load for detecting the inner and outer boundaries of an iris while improving the detection rate if approximation components are used without rescaling. In other words, the proposed method cannot only make the computations more efficient but also improve

the correct location ratio at the same time. The experiments prove that the idea of the proposed method is quite feasible.

A normalized iris image is the input image of the feature extraction stage. Normalization algorithm has been implemented for many iris databases such as CASIA, MMU, etc. Since the normalized iris image has relatively low contrast and may have non-uniform intensity values due to the position of the light sources, a local intensity-based histogram equalization technique is applied to enhance the quality of the contrast of the normalized iris image, thereby increasing the subsequent recognition accuracy.

CHAPTER 4

Feature Extraction using Three Level Haar Wavelet Transform and Modified Local Binary Pattern

4.1 Overview

Iris recognition has several applications in security systems of banks, border control, restricted areas, etc., [35-37]. One key part of such a system is the extraction of prominent texture information or features in the iris. This feature extraction method generates feature vectors or feature codes. The feature vectors of the unknown images are used to match those of the stored known ones. In an iris recognition system, the matching process matches the extracted feature code of a given image with the feature codes previously stored in the database. In this way, the identity of the given iris image can be known. Despite significant research results so far [3, 31, 37-44], there are several challenges in iris recognition [45-57]. One problem is the occlusion, i.e., the hiding of the iris caused by eyelashes, eyelids, specular reflection, and shadows [53]. Occlusion can introduce irrelevant parts and hide useful iris texture [53]. Another issue is the computation time of iris identification. For large population sizes, the matching time of iris can sometimes become exceedingly high for real-time applications, and the identification delay increases with the increase in the population size and the length of feature codes. It has been reported in the recent literature [46, 48, 49] that the existing iris recognition methods still suffer from long run times apart from other factors. This is particularly true when the sample size is very large, and the iris images are non-ideal and captured from different types of cameras. Hence, devising a method that reduces the run time of iris recognition without compromising accuracy is still an important research problem. The identification delay can be reduced by reducing the feature vector of iris images. Thus, this chapter focuses on the issue of reducing the feature vector, which will lead to a reduction in identification delay without lowering the identification accuracy. For lowering the feature vector, the concept of Haar wavelet along with a modified local binary pattern (MLBP) is used in this work. Note that in the context of face recognition [58-61] and fingerprint identification [62], the Haar wavelet transform demonstrates an excellent recognition rate at a low computation time. In [63], the Haar wavelet is also proposed without the use of MLBP.

In this chapter, a feature extraction method is proposed for faster iris recognition. This new method is a hybrid process combining three-level HWT and MLBP. In this hybrid method, firstly, HWT is applied to the normalized iris image resulting in four output images, including the approximation image known as LL sub-band. This LL sub-band is then further decomposed using HWT into four sub-images. The resultant second-level LL is decomposed using HWT into the third-level LL sub-band. The application of repeated HWT extracts the major information containing region, reducing the information size. Next, MLBP is applied to the obtained LL, where MLBP includes LBP and XOR operations. The output of MLBP is a binary iris template. The effectiveness of this proposed hybrid HWT-MLBP method is experimentally evaluated using three different datasets.

4.2 Literature Review

A number of research papers describe iris feature extraction techniques which are discussed in the following.

Ma et al. [37] applied a bank of spatial filters to acquire local details of the iris. These spatial filters generate discriminating texture features for an iris image based on the characteristics of the iris. Ma et al. [38] considered a bank of circular symmetric filters for iris feature extraction. These filters [38] are modulated by a circular symmetric sinusoidal function which is different from the Gabor filter modulated by an orientated sinusoidal function. Monroe et al. [39] used discrete cosine transform (DCT) for iris recognition. Daugman [3] introduced the idea of using a 2-D Gabor wavelet filter for extracting features of an iris image. Furthermore, Masek et al. [31] used 1-D and 2-D Log-Gabor filters for feature extraction. Li et al. [40] used a convolutional neural network (CNN) algorithm, which is a form of deep learning to extract iris features. Umer et al. [41] used a novel texture code defined over a small region at each pixel. This texture code was developed with a vector order based on the principal component of the texture vector space. Soliman et al. [42] considered feature extraction using the Gabor filter, where the original Gabor features were masked via a random projection scheme. The masking was performed to increase the level of security. In this scheme, the effects of eyelids and eyelashes were removed. An iris feature extraction method using wavelet based 2D mel-cepstrum was proposed in [44] where cepstrum of a signal is the inverse Fourier transform of the logarithm of the

estimated signal spectrum. This scheme applied *Cohen-Daubechies-Feauveau* (CDF) 9/7 filter bank for extracting features. In wavelet cepstrum, non-uniform weights are assigned to the frequency bins. In this way, the high frequency components of the iris image are emphasized resulting in greater recognition reliability. Furthermore, this wavelet cepstrum method helps to reduce the feature set.

Barpanda et al. [45] used a tunable filter bank to extract region-based iris features. These filters were used for recognizing non-cooperative images instead of high-quality images collected in cooperative scenarios. The filters in this filter bank were based on the half band polynomial of 14th order, where the filter coefficients were extracted from the polynomial domain. To apply the filter bank, the iris template was divided into six equi-spaced parts, and the features were extracted from all the parts except the second one, which mainly contains artifacts. Betancourt et al. [46] proposed a robust key-points-based feature extraction method. To identify distinctive key-points, three detectors, namely Harris-Laplace, Hessian-Laplace, and Fast-Hessian were used. This method is suitable for iris recognition under variable image quality conditions.

For iris feature extraction, Saha et al. [48] used *phase intensive local pattern* (PILP), which consists of density-based spatial clustering and key-point reduction. This technique groups some closely placed key-points into a single key-point leading to high-speed matching. Jamaludin et al. [49] used 1D log-Gabor filter and considered the sub-iris region for feature extraction. This filter has a symmetrical frequency response on the log axis. In this case, only the lower iris regions that are free from noise, as well as occlusions, are considered.

In [50], combined *discrete wavelet transform* (DWT) and DCT were used for the extraction of iris features. Firstly, DWT was performed where the output of this stage was in the spatial domain. Next, DCT was performed to transform the spatial domain signal to the frequency domain and to obtain better discriminatory features. Another feature extraction method is the discrete dyadic wavelet transform reported in [51]. In dyadic wavelet transform, the decomposition at each level is done in a way that the bandwidth of the output signal is half of the input. In [52], a phase intensive local pattern (PILP) technique is used for feature extraction and to obtain a feature vector of 1×128 . In this PILP method, there are four stages named keypoint detection via phase intensive patterns, removal of edge features, computation of oriented histogram and formation of a feature vector. Iris features were extracted using 1-D DCT and

relational measure (RM), where RM encodes the difference in intensity levels of local regions of iris images [53]. The matching scores of these two approaches were fused using a weighted average. The score-level fusion technique compensates for some images that are rejected by one method but accepted by the other [53]. Another way of extracting feature vectors from iris images is the use of linear predictive coding coefficients (LPCC) and linear discriminant analysis (LDA) [54]. Llano et al. [57] used a 2D Gabor filter for feature extraction. Before applying this filter, a fusion of three different algorithms was performed at the segmentation level (FSL) of the iris images to improve the textual information of the images. Oktiana et. al. [64] proposed an iris feature extraction system using an integration of Gradientface-based normalization (GRF) where GRF uses an image gradient to remove the variation in illumination level. Furthermore, the work in [64] concatenated the GRF with a Gabor filter, a difference of Gaussian (DoG) filter, binary statistical image feature (BSIF), and LBP, for iris feature extraction in a cross-spectral system. Shuai et al. proposed [65] a iris feature extraction method based on multiple source feature fusion performed by a Gaussian smoothing filter and a texture histogram equalization. Besides, there have been some recent studies in the field of iris recognition [66-75], where some focus on iris feature extraction methods [67-72] and some on iris recognition tasks [73-75].

A summary of some of the most relevant works on iris feature extraction is shown in Table 4.1.

Table 4.1: Summary of literature review

Ref.	Adopted Technique	Remarks	Database
[37]	Spatial filters constructed based on observations	Features are extracted only in the upper portion of the normalized iris image as it provides useful texture information. The feature vector length is large, being 1x1536.	CASIA-Iris-V1
[38]	A bank of circular symmetric filters	The top-most 75% of the unwrapped iris images are used for texture information. The variation of the texture of the iris in the local region is not focused on in this paper.	

Ref.	Adopted Technique	Remarks	Database
[39]	Patch Coding technique for extracting fast Fourier transformation (FFT) based features from normalized iris images	The method has low complexity with high accuracy. The dimensionality of the feature vector is 1x 2343. However, non-ideal images are not considered.	CASIA-Iris-V1
[3]	2D Gabor filter	The dimensionality of the feature vector is 1x2048.	
[31]	1D and 2D Log-Gabor filters	This method cannot produce features of different frequencies, and the size of the iris template is 1×4800.	CASIA-Iris-V1
[40]	Deep learning	CNN as deep learning is used to extract iris features, and the features are then used for image encryption.	CASIA-Iris-V4
[41]	Texture code co-occurrence matrix	Feature vector size 1x400. The method uses only part of the iris images to avoid occlusion caused by eyelashes and eyelids.	UPOL, CASIA-Iris-V3 Interval, MMU1 and IITD,
[42]	1D Gabor filter where Gabor features are masked	Masks the original Gabor features to increase the level of security while excluding eyelids and eyelashes' effects. Moreover, considers only the upper half of the normalized iris portion.	CASIA-Iris-V3-Interval
[43]	2D kernel and hybrid MLPNN-PSO algorithm	Feature extraction is performed on a small sample of 140 images at an accuracy rate of 95.36%. In this case, 1000 iterations are performed, which leads to high computational time.	CASIA-Iris-V3
[44]	2D wavelet cepstrum technique for feature extraction	False acceptance rate is 10.45%, recognition accuracy is 89.93%.	CASIA-Iris-V3 , UBIRISv1, IITD
[45]	Tunable filter bank based on half band polynomial of 14th order	The false acceptance rate is 8.45%, recognition accuracy is 91.65%.	CASIA-V3 , UBIRISv1, IITD

Ref.	Adopted Technique	Remarks	Database
[46]	Key-points based feature extraction method	Considers only salient key points in the whole region. The feature extraction stage is time-consuming.	CASIA-Iris-V4-Interval, MMU 2, UBIRIS 1
[48]	Density-based spatial clustering and key-point reduction to be applied on PILP	For feature extraction and feature vector reduction, post-processing is required leading to additional time consumption.	BATH and CASIA-Iris-V3
[49]	Sub-iris Technique	Does not extract features of the unoccluded upper part of the iris region.	CASIA-Iris-V4
[51]	Discrete dyadic wavelet transform	Iris images of only 10 people are used, and a feature vector of 1×256 is achieved. Results need to be validated with a higher number of subjects.	
[52]	local feature based on phase intensive patterns	Feature extraction is based on keypoint detection via phase-intensive patterns. Obtains a feature vector of 1×128 .	BATH, CASIA-Iris-V3, UBIRISv2, and FERETv4
[53]	DCT and RM	Based on the dissimilarity score of DCT and RM and using the Hamming distance metric, the matching of images is performed. This is used to compensate for images rejected by either DCT or RM but accepted by the other.	CASIA-Iris-V4 Interval, Lamp, and self-collected IITK
[54]	LPCC and LDA	The method has high complexity, and for the case of LPCC, the feature vector results in 1×546 dimension	CASIA-Iris-V1
[57]	Textural information development and exploration	This method has three stages: quality evaluation, automatic segmentation, and fusion at the segmentation level. This method rejects images having low quality. The obtained feature vector is 1×2048 .	MBGC-V2, CASIA-Iris-V3, CASIA-Iris-V4 and UBIRIS v1 (for iris image)

Ref.	Adopted Technique	Remarks	Database
[64]	Gabor filter, a DoG filter, BSIF, and LBP	The feature extraction is done using the fusion of GRF with a Gabor filter, a DoG filter, a BSIF, and LBP. Hamming distance is used for matching purposes.	Hong Kong Polytechnic University Cross-Spectral Iris Images Database
[65]	Convolutional neural network	Feature extraction is done using the concept of feature fusion which is achieved by a Gaussian filter and a texture histogram equalizer.	JLU iris library

4.3 The Proposed Feature Extraction Scheme

This section describes the proposed iris feature extraction method. Fig. 4.1 represents the block diagram of the proposed three-level HWT and MLBP. The decomposition of the image three times by HWT results in the reduction in feature size without significant loss in the image quality or important attributes. The use of MLBP further reduces the feature vector size without a loss in image attributes. Fig. 4.2 shows the three-level HWT. It can be seen from the figure that at each level of HWT, the input image is divided into four output images. These output images are denoted as *horizontal detail* (HL), *vertical detail* (VL), *diagonal detail* (HH), and *approximation* (LL) images. The LL subimage, also known as LL subband, contains the significant information of the original image. In other words, the LL subband is a coarse approximation of an image, and it does not contain high-frequency information. Next, the three-level HWT algorithm is discussed.

Algorithm 1: HWT**Input:** Normalized iris image**Output:** Approximation part of level three**Main Process:**

Step 1: Apply first level HWT to the normalized iris image to generate its wavelet coefficients.

Step 2: Apply second level HWT on the approximation part obtained from Step 1 to generate its wavelet coefficients.

Step 3: Apply third level HWT on the approximation part obtained from Step 2 to generate its wavelet coefficients.

Step 4: Get the level three approximation part obtained from Step 3.

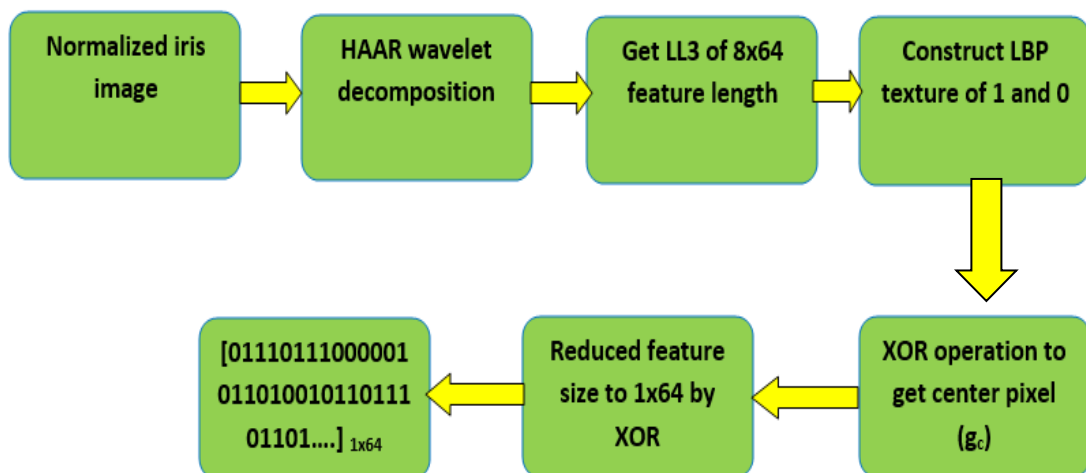


Fig. 4.1: Block diagram of the proposed approach for iris feature extraction.

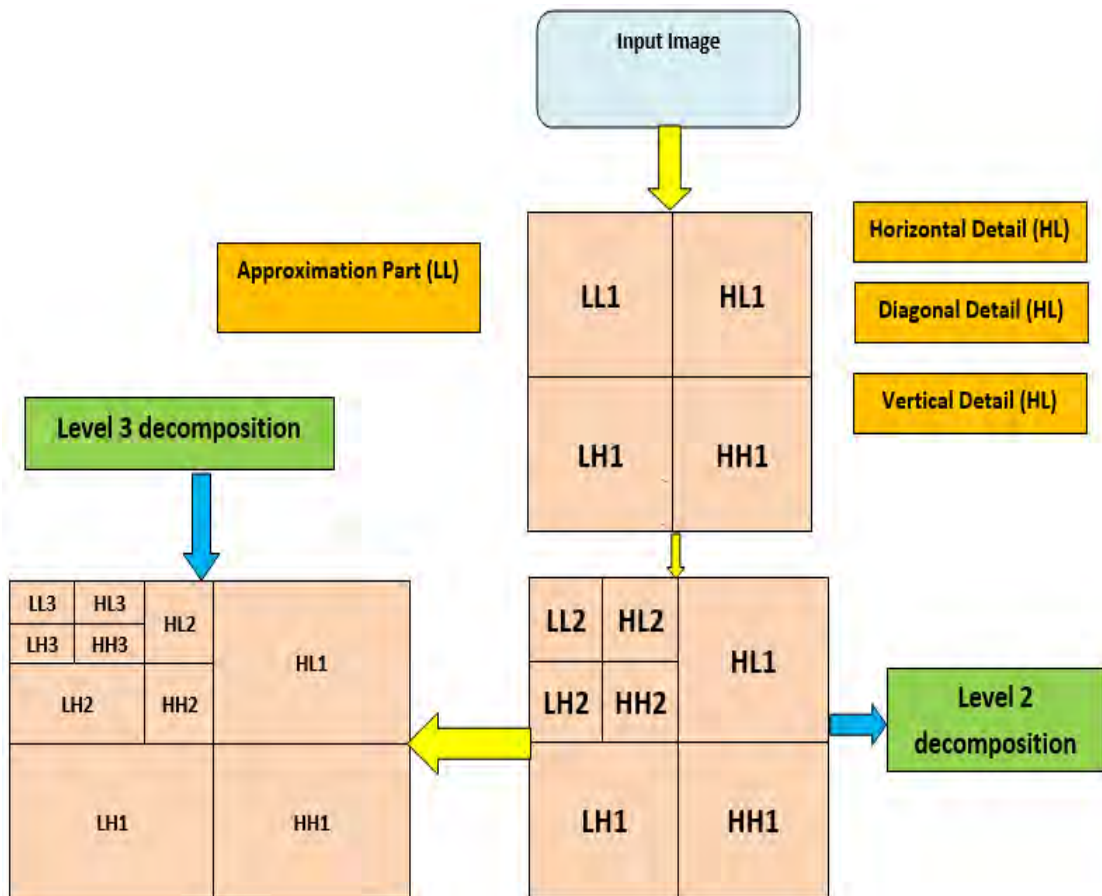


Fig. 4.2: Three-level HWT

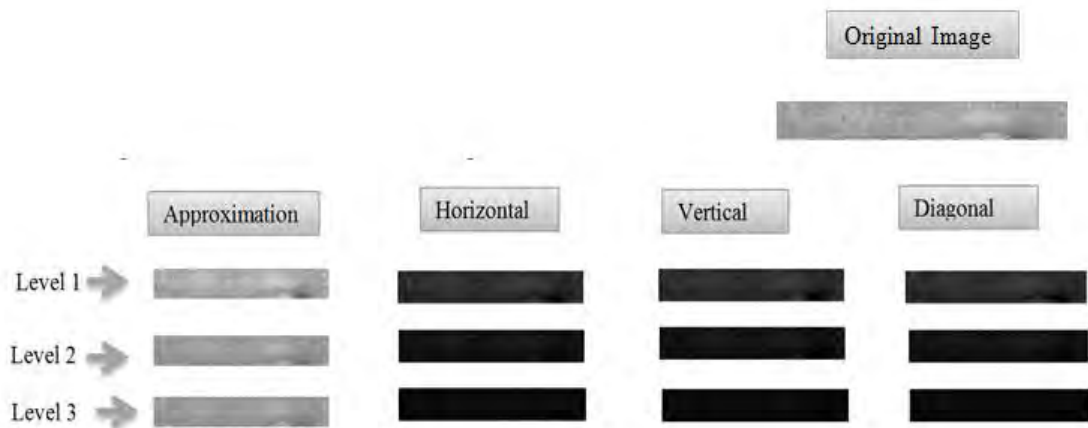


Fig. 4.3: Three-level wavelet decomposition of normalized iris

The main idea of using HWT is that wavelet decomposition can transform a detailed image into approximation images. The approximation parts contain a major portion of the energy of the images. The HWT is repeatedly executed to shrink the information size. The results of the three-level decomposition produce a reduced

characteristics region having little loss. This is shown in Fig. 4.3. It can be noted that most of the information of the iris image is contained in the extracted LL (low frequency) region on the multi-divided iris image, as indicated by Fig. 4.3. The other regions have less information, as indicated by their low intensity (dark) levels. Fig. 4.4 illustrates the size of each level for the three-level HWT. The application of level-1 HWT to the normalized image of size 64×512 results in wavelet coefficients of $LL1$, $LH1$, $HL1$, and $HH1$. In this case, the approximation part of level 1 denoted as $LL1$ becomes of size 32×256 . Next, level 2 HWT is applied to $LL1$, which generates wavelet coefficients of $LL2$, $LH2$, $HL2$, and $HH2$. In this case, the approximation part of level 2 ($LL2$) becomes of size 16×128 . After that level-3 HWT is applied to $LL2$ to generate its wavelet coefficients $LL3$, $LH3$, $HL3$, and $HH3$. In this case, the approximation part of level 3 ($LL3$) becomes of size 8×64 . Hence, a major distinctive region, $LL3$ is obtained by performing the wavelet transformation three times. Next, $LL3$ region is used for the MLBP tasks.

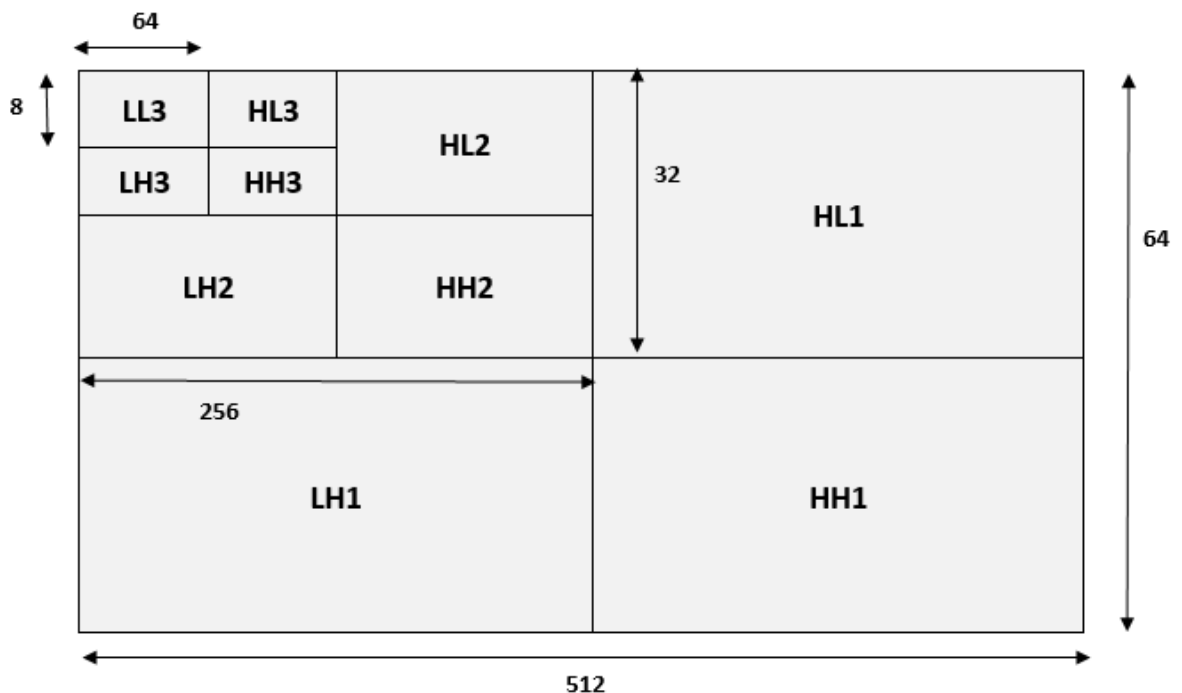


Fig. 4.4: Three-level HWT with the size of each level

Now, consider the MLBP operation [55], which generates robust binary features. Furthermore, MLBP has low computational complexity. MLBP labels each pixel based on the neighbouring pixels and considers a given threshold. MLBP then produces outputs in the binary format. This binary code can describe the local texture pattern. Note that MLBP is an LBP followed by an XOR operation. Next, MLBP operation is described in the following.

For a center pixel c , and neighboring pixels p within a neighborhood of P pixels, the MLBP operation can be expressed as follows.

$$LBP_p = \sum_{p=0}^{P-1} S(g_p - g_c) \times 2^p \quad (1)$$

Where, LBP_p is the MLBP operator, g_c is the gray level of c and g_p is the gray level of p pixels. Moreover, $S(x)$ in (1) refers to the sign function defined as,

$$S(x) = \begin{cases} 1 & \text{if } x \geq 0 \\ 0 & \text{otherwise} \end{cases} \quad (2)$$

Next, the center pixel value is generated by applying XOR operation on the values of LBP_p . This results in the following expression.

$$\psi_{\oplus}(s_p) = s_0 \oplus s_1 \oplus \dots \oplus s_{P-1} \quad (3)$$

Where \oplus denotes the XOR operator and $\psi_{\oplus}(s_p)$ is the binary iris code obtained as XOR output. Since it is a commutative operation of XOR, this can be performed by circularly shifting on s_p in clockwise or anticlockwise. Now XOR is performed to reduce the size from 8×64 to 1×64 . XOR is computed in the column vector. In other words, 8-row iris signature is reduced to a single row only. Fig. 4.5 and Fig. 4.6 describe the MLBP operation. Fig. 4.5 shows the center pixel in a 3×3 neighborhood, while Fig. 4.6 illustrates the computation of $LBP_{8,1}$ with XOR for a single pixel.

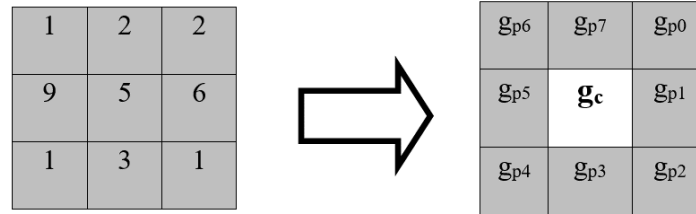


Fig. 4.5: Center element of a 3x3 pixel image

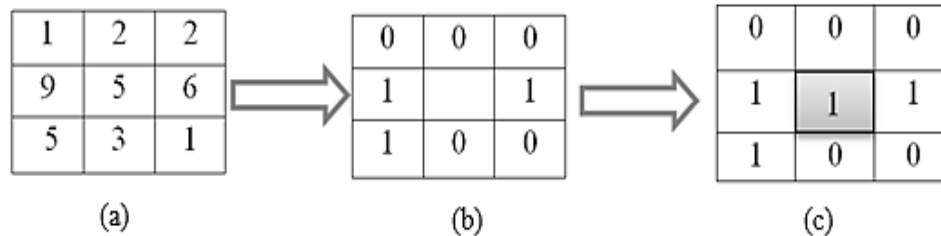


Fig. 4.6: MLBP operation of 3x3 sub region: (a) the neighborhood of a pixel within the image, (b) the threshold version of the neighbourhood, (c) MLBP pattern where the middle pixel has been computed.

Algorithm 2: Feature encoding using the proposed MLBP

Input: Level three approximation part of the normalized image

Output: Binary sequence of the normalized iris image.

Main Process:

Step 1: Read the intensity values of the level three approximation part of the normalized image.

Step 2: Convert the RGB image to grayscale form

Step 3: Resize the image if required and then store the size $[M, N]$ of the image

Step 4: Divide the image into 8 segments.

Step 5: For each of the image segments, apply a 3×3 kernel

Step 6: Get the list of neighbourhood pixels, P

Step 7: Loop through each neighbourhood pixel in the image

Step 8: Take the center pixel (g_c) and set it as a threshold for its P neighbors.

Step 9: Compute the difference pixel value after finding out the difference between neighbouring pixels and centre pixels

Step 10: If the difference pixel value is less than zero, then set the sign function value of that neighbouring pixel to zero. Otherwise, set the sign function value to 1.

Step 11: End of loop.

Step 12: Apply the XOR operation of the sign function output to get the binary mask.

Step 13: Place the binary output of the XOR operation in the center pixel.

Step 14: Move the kernel in order to obtain a binary template.

Step 15: Apply XOR operation across the columns.

So, for the case of MLBP, the first LBP operation extracts the distinctive features to generate a unique iris code. This code is reduced from 8×64 features to 1×64 by applying the XOR operation.

4.4 Summary

Iris feature extraction is an important aspect of many modern security systems. Hence, an efficient and faster approach is important for iris recognition. This chapter proposes a new hybrid HWT and MLBP based technique to reduce feature size so that the iris images can be matched faster. HWT extracts the most prominent features of the iris, reducing the template size. In this work, a three-level HWT is applied to extract the region containing the major information of the iris image. The three-level approximation part resulting from HWT is considered as a major characteristics region. For instance, the repeated HWT converts a 64×512 normalized iris image into an approximation image of 8×64 which becomes a template of 1×64 after the application of MLBP and XOR. The proposed hybrid HWT and MLBP algorithm are applied on three different iris datasets.

CHAPTER 5

LBPX: A Novel Feature Extraction Method for Iris Recognition

5.1 Overview

Iris recognition is a means of biometric identification. A key part of the recognition system using the iris is the extraction of prominent texture information or features in the iris. The identification delay in iris recognition can be reduced by reducing the feature vector generated from the feature extraction of iris images. A new form of LBP termed LBPX is proposed in this thesis as an iris feature extraction method. For this, input eye images are processed and converted to normalized iris images employing circular Hough transformation and Daugman's rubber sheet model. Next, LBPX is applied to the normalized images. In this LBPX stage, rotation-invariant LBP operation takes place. The performance of LBPX based recognition system adopting iris image is evaluated in terms of accuracy and feature vector length. This is done for three datasets CASIA-IRIS-V4, UBIRIS, and IITD.

5.2 Literature Review

Several research papers describe iris feature extraction methods. The work in [38] used a bank of special filters with parameters modulated by circular and symmetric sinusoidal functions to extract the features of the iris image. Ma et al. [37] applied a bank of spatial filters to acquire local details of the iris. These spatial filters generate discriminating texture features for an iris image based on the characteristics of the iris. Mohammad AE Abdalla et al. [76] provided a method in order to analyze the amalgamation of the iris features extracted by DWT and DCT all at once. They used CASIA interval-V4 as an image database and multiclass SVM to classify the iris patterns [76]. Discrete cosine transform (DCT) was also applied to recognize the iris template of a person [39]. Younghui Wang applied Hough transform to find the iris' inner and outer boundaries of the iris and then normalized the segmented iris image [77]. The db4 wavelet was used with Shannon entropy to decompose that normalized iris image and extract the important features from the decomposed image. Hamming

distance had been used for matching purposes [77]. Hammou Djalal Rafik et al. adopted Hough Transform for achieving the segmented iris image and 1D Log-Gabor filter for extracting the iris features from the segmented image [78]. They had also used Hamming distance for determining the authenticity of the person's identity [78]. Amina A. abdo et al. [79] proposed an iris recognition system on the CASIA interval-V4 iris image database combining histogram equalization and DCT to capture the iris' discriminative features. Thiri Kyaw used Sobel edge operating to detect the iris edges and statistical correlation technique based on skewness and entropy to obtain less execution time [80]. Adamović et al. [81] applied the Base64 encoding algorithm for transforming a normalized iris segment into a template having stylometric-based features and then applied different machine learning models for performance evaluation. Muktar Danlami et al. [82] applied Gabor filter and Legendre wavelet filters on the processed image of three different datasets such as CASIA, MMU, and UBIRIS for extracting the unique feature of the segmented iris image in order to recognize the person's identity. They evaluated and compared their proposed model based on the FRR, FAR, GAR (Genuine Acceptance Rate), and accuracy. Their result showed that the Legendre wavelet filter's recognition accuracy is comparatively better than the Gabor filter for the UBIRIS image database. Chen et al. applied DCT and Gabor wavelet on the segmented iris images collected from the CASIA image database to perform the iris localization and iris extraction stage [75]. Finally, Euclidean distance and the nearest neighbor distance detector were used as classifiers in the iris recognition system [75]. Lasker Ershad Ali et al. [83] proposed a novel approach by applying RW (random walker) algorithm for segmenting the coarse iris segmentation in order to achieve the iris image with its corresponding binary mask and by utilizing Log-Gabor wavelet-based Contourlet transform (LGCT) feature descriptor with kernel-based extreme learning machine (KELM) classifier. CASIA-v4 database was used in [84]. Oluwakemi Christiana Abikoye et al. [85] addressed a comparative analysis of three feature extraction methods. These schemes include Gabor/Haar Wavelet Transform and Scale Invariant Feature Transform (SIFT) applied to CASIA iris dataset. They declared in their experimental results that Gabor Wavelet method outperformed the other two methods in terms of training time, testing time, and recognition accuracy. The study in [31] performed feature extraction using 1-D and 2-D Log-Gabor filters. Li et al. [40] reported the use of the convolutional neural network (CNN), while Umer et al. [41] used a texture code defined for each

pixel on a small region. Soliman et al. [42] removed eyelids and eyelashes and then masked the features obtained at the output of a Gabor filter.

5.3 Methodology

This section describes the LBPX method used in this thesis. The experiment was conducted on images collected from IITD [86], CASIA-IrisV1 (756 iris images of resolution 320x280 from 108 eyes) [87], and CASIA-IrisInterval [84]. After performing iris image pre-processing, iris segmentation, and iris normalization, LBPX was applied to extract the feature of the normalized iris image. Firstly, pre-processing was performed. As part of pre-processing, iris edge detection and noise removal were performed [88]. In this experiment, the Canny operator was applied to find the edges considering the image gradients. Then the operator focuses on local maxima. After that, a threshold value was applied by the operator for discovering the potential edge. In order to remove any unwanted noise, various basic filters were used [89]. In the iris segmentation stage, Hough transform was applied in finding the boundaries (inner as well as outer) and next to find the areas of the eyelids and eyelashes. In the normalization stage, Daugman's Rubber Sheet model was used in this case. The segmented iris images were transformed from the radial co-ordinate axis to the rectangular, polar co-ordinate axis to sustain the size invariance or translation invariance. LBPX was introduced in the feature extraction stage. LBPX is a gray scale and rotation invariant texture operator. This operator was derived by focusing the joint distribution of gray values within a circularly symmetric neighbour set of pixels. The proposed LBPX approach can be considered as a robust method in terms of gray scale variations due to the invariance property of the operator against any monotonic transformation of the gray scale. The gray scale-invariant operator can also integrate a specified set of rotation invariant patterns [90-93].

The proposed LBPX is a combination of the concepts of uniform LBP, rotation-invariant LBP, and XOR operators. Firstly, the concept of a uniform LBP operator is discussed. A uniform LBP operator is a generalized grayscale scheme developed to extract certain binary texture T. These are fundamental features of the iris image and have a uniform look as there are limited discontinuities on the circular patterns. The uniform LBP operator detects the patterns at the circular neighbourhood of the

angular space. Uniform LBP operator can be denoted as $LBP_{Q,R}$ where Q indicates the circularly symmetric member set and the quantization factor of the angular space, and radius R of the circle indicates the spatial resolution. The term $LBP_{Q,R}$ can be expressed as

$$LBP_{Q,R} = \sum_{q=0}^{Q-1} V(g_q - g_c) \times 2^q \quad (5.1)$$

where $V()$ is the sign function, the term g_c is the gray value of the pixel placed at the center, g_q indicates the gray values of Q number of pixels that are placed at equal distance on the circle circularly symmetric neighbour set. The $LBP_{Q,R}$ is constant against any monotonic transformation of gray values of the images. The operator $LBP_{Q,R}$ generates 2^Q output values for $2Q$ binary patterns for the case of P pixels. For rotated images, the term g_q moves circularly around g_0 . When a binary pattern is rotated, a different $LBP_{Q,R}$ value is generated. However, when the pattern has only 1's or only 0's, the different $LBP_{Q,R}$ value remains constant irrespective of the rotation. The rotation invariant LBP operator $LBP_{Q,R}^{ri}$ can be expressed as,

$$LBP_{Q,R}^{ri} = \min\{ROR(LBP_{Q,R}, n) \mid n = 0, 1, \dots, Q - 1\} \quad (5.2)$$

where $ROR(y, n)$ is the circular shift on the right side of Q -bit number, and y n means the number of shifts. As the formal definition of 'uniform' patterns, a uniformity measure $U(\text{'pattern'})$ has been introduced, which indicates the number of bitwise changes known as transitions in space.

$$LBP_{Q,R}^{riu2} = \begin{cases} \sum_{q=0}^{Q-1} V(g_q - g_c) & \text{if } U(LBP_{Q,R}) \leq 2 \\ Q + 1 & \text{otherwise} \end{cases} \quad (5.3)$$

where,

$$U(LBP_{Q,R}) = |V(g_{Q-1} - g_c) - V(g_0 - g_c)| + \sum_{q=1}^{Q-1} |V(g_q - g_c) - V(g_{q-1} - g_c)| \quad (5.4)$$

In $LBP_{Q,R}^{riu2}$, the superscript $riu2$ is the rotation invariant 'uniform' pattern which has a maximum at most of 2. It can be noted that $Q+1$ 'uniform' binary patterns exist. After

incorporating the uniform and rotation invariant LBP concepts, the proposed LBPX operator calculates XOR operation through its column vector.

5.4 Summary

This chapter describes a novel feature extraction method termed LBPX. This LBPX is a combination of the ideas of uniform LBP, rotation-invariant LBP, and an XOR method followed by LBP operations. The proposed method leads to a smaller feature vector size compared to existing methods, including RIU LBP.

CHAPTER 6

Matching and Distance Measurement

6.1 Overview

After extracting the features applying discrete wavelet transforms or local binary patterns, the normalized iris image is transformed into a unique representation within the feature vector. In order to obtain the acceptance and refusal rate, a distance is calculated to measure the close-ness of an iris pattern match. The template that is generated in the feature encoding process will also need a corresponding matching metric, which gives a measure of similarity between two iris templates. This metric should give one range of values when comparing templates generated from the same eye, known as intra-class comparisons, and another range of values when comparing templates created from different irises, known as inter-class comparisons. These two cases should give distinct and separate values so that a decision can be made with high confidence as to whether two templates are from the same iris, or from two different irises.

6.2 Hamming Distance

The Hamming distance gives a measure of how many bits are the same between two-bit patterns. Using the Hamming distance of two-bit patterns, a decision can be made as to whether the two patterns were generated from different irises or from the same one.

In comparing the bit patterns X and Y , the Hamming distance, HD , is defined as the sum of disagreeing bits (sum of the exclusive-OR between X and Y) over N , the total number of bits in the bit pattern.

$$HD = \frac{1}{N} \sum_{i=1}^N X_i(XOR)Y_i \quad (6.1)$$

Since an individual iris region contains features with high degrees of freedom, each iris region will produce a bit-pattern that is independent of that produced by another

iris. On the other hand, two iris codes produced from the same iris will be highly correlated.

If two bits patterns are completely independent, such as iris templates generated from different irises, the Hamming distance between the two patterns should equal 0.5. This occurs because independence implies the two-bit patterns will be totally random, so there is a 0.5 chance of setting any bit to 1 and vice versa. Therefore, half of the bits will agree, and half will disagree between the two patterns. If two patterns are derived from the same iris, the Hamming distance between them will be close to 0.0 since they are highly correlated, and the bits should agree between the two iris codes.

The Hamming distance is the matching metric employed by Daugman, and calculation of the Hamming distance is taken only with bits that are generated from the actual iris region. Two iris templates generated from the same iris will have a Hamming distance of 0.0; in practice, this will not occur. Normalization is not perfect, and also, there will be some noise that goes undetected, so some variation will be present when comparing two intra-class iris templates.

In order to account for rotational inconsistencies, when the Hamming distance of two templates is calculated, one template is shifted left and right bit-wise, and a number of Hamming distance values are calculated from successive shifts. This bit-wise shifting in the horizontal direction corresponds to rotation of the original iris region by an angle given by the angular resolution used. If an angular resolution of 180 is used, each shift will correspond to a rotation of 2 degrees in the iris region. This method is suggested by Daugman [3, 4, 7] and corrects for misalignments in the normalized iris pattern caused by rotational differences during imaging. From the calculated Hamming distance values, only the lowest is taken since this corresponds to the best match between two templates.

The number of bits moved during each shift is given by two times the number of filters used, since each filter will generate two bits of information from one pixel of the normalized region. The actual number of shifts required to normalize rotational inconsistencies will be determined by the maximum angle difference between two images of the same eye, and one shift is defined as one shift to the left, followed by one shift to the right. The shifting process for one shift is illustrated in Fig. 6.1. One

shift is defined as one shift left and one shift right of a reference template. In this example, one filter is used to encode the templates, so only two bits are moved during a shift. The lowest Hamming distance, in this case, zero, is then used since this corresponds to the best match between the two templates.

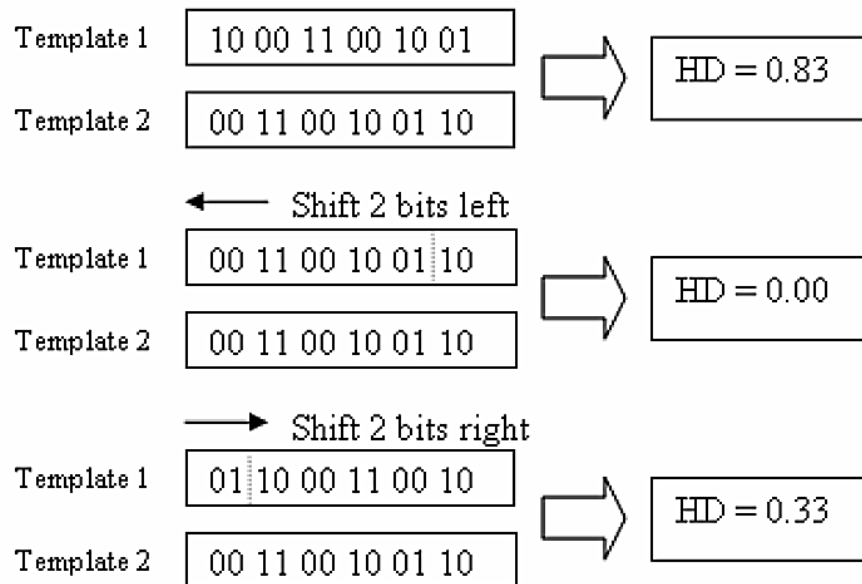


Fig. 6.1: An illustration of the shifting process.

6.3 Experimental Results

Figs. 6.2 and 6.3 illustrate the unmatched and matched condition respectively. For unmatched conditions, the obtained hamming distance is 0.4632. On the contrary, for the matched condition, the achieved hamming distance is 0.2455 since the threshold value of 0.28 is selected in this case.

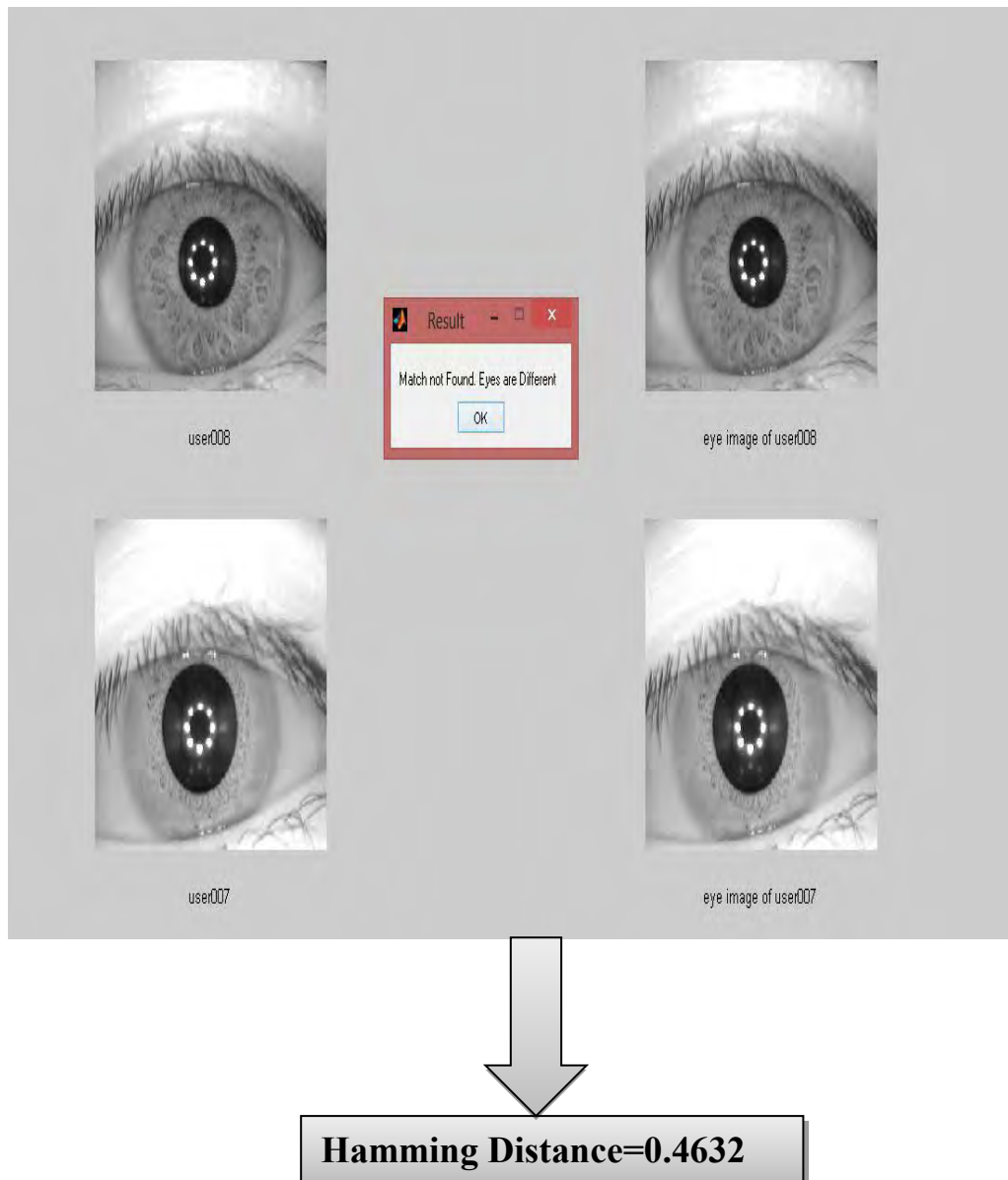


Fig. 6.2: Unmatched Conditions

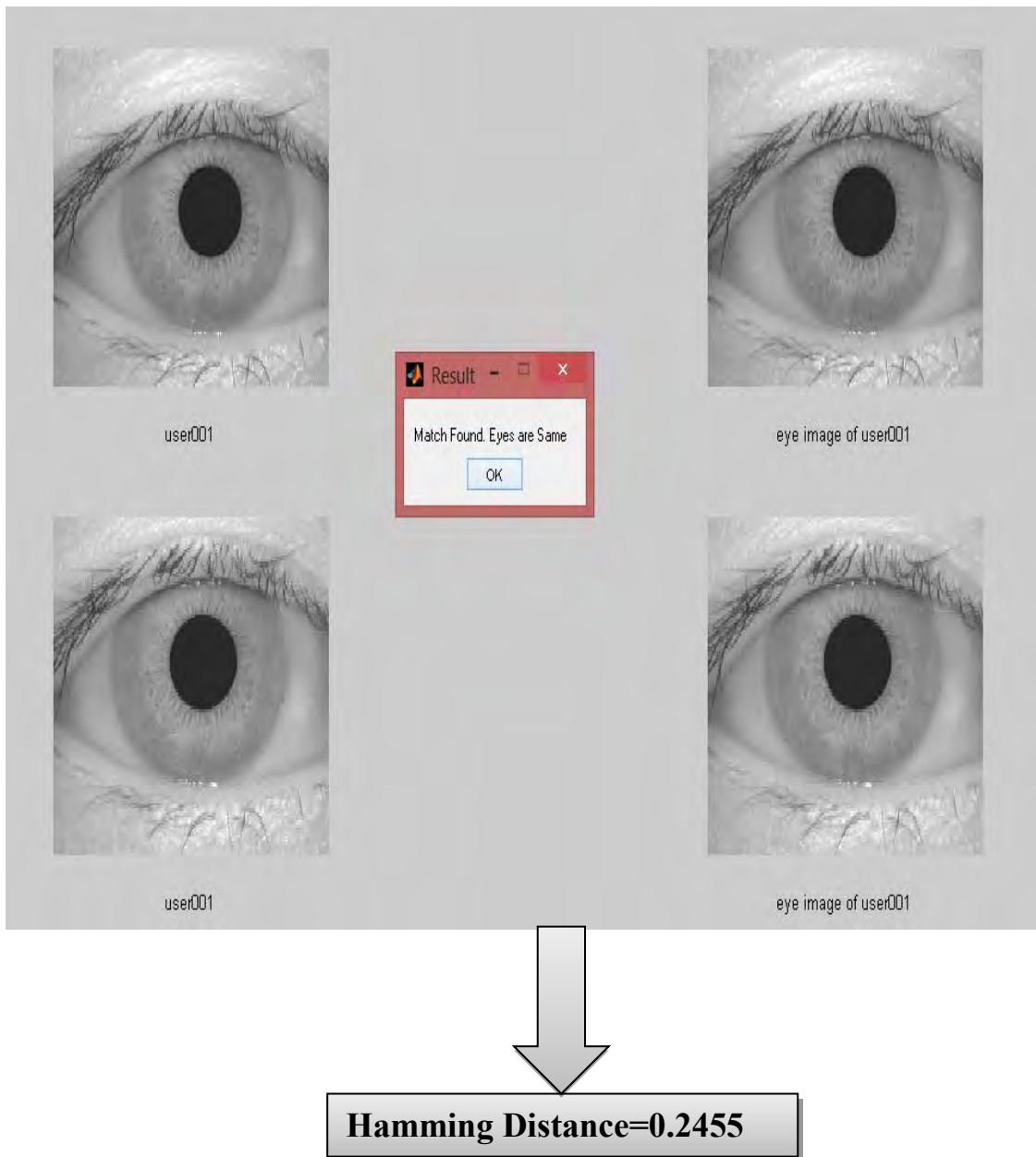


Fig. 6.3: Matched Condition

CHAPTER 7

Experimental Result and Analysis

7.1 Overview

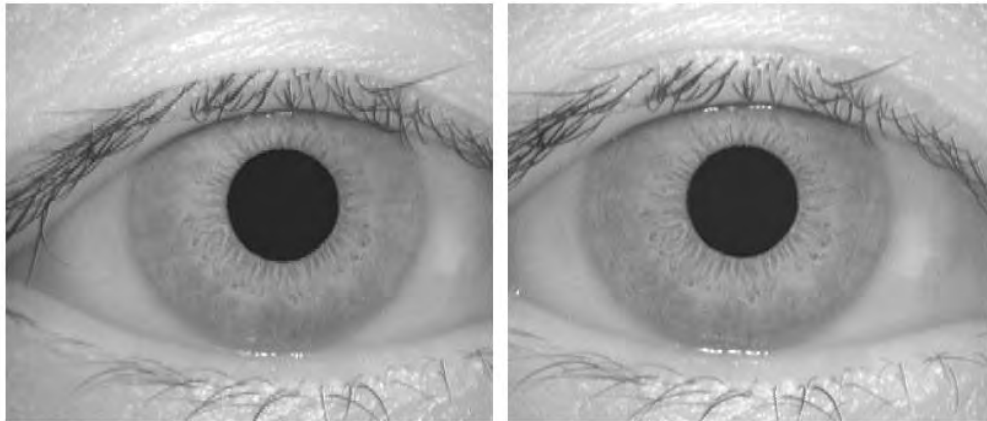
In this chapter, the performance of the iris recognition system as a whole is examined. Tests were carried out to find the best separation so that the false match and false accept rate is minimized and to confirm that iris recognition can perform accurately as a biometric for recognition of individuals. As well as confirming that the system provides accurate recognition; experiments were also conducted in order to confirm the uniqueness of human iris patterns by deducing the number of degrees of freedom present in the iris template representation. There are a number of parameters in the iris recognition system, and optimum values for these parameters were required in order to provide the best recognition rate.

7.2 Datasets

7.2.1 Chinese Academy of Sciences - Institute of Automation (CASIA)

CASIA Iris Image Database Version 1.0 (CASIA-IrisV1) includes 756 iris images from 108 eyes. For each eye, 7 images are captured in two sessions with our self-developed device CASIA close-up iris camera, where three samples are collected in the first session and four in the second session. Fig. 7.1 represents the sample images CASIA-IrisV1. All images are stored in BMP format with resolution 320*280[87].

CASIA-IrisV4 is an extension of CASIA-IrisV3 and contains six subsets. The three subsets from CASIA-IrisV3 are CASIA-Iris-Interval, CASIA-Iris-Lamp, and CASIA-Iris-Twins, respectively[84]. The three new subsets are CASIA-Iris-Distance, CASIA-Iris-Thousand, and CASIA-Iris-Syn. CASIA-IrisV4 contains a total of 54,601 iris images from more than 1,800 genuine subjects and 1,000 virtual subjects. All iris images are 8 bit gray-level JPEG files, collected under near-infrared illumination or synthesized. Fig. 7.2 represents the iris images of CASIA-Iris-Interval.



(a) Session1

(b) Session2

Fig. 7.1: Example iris images in CASIA-IrisV1

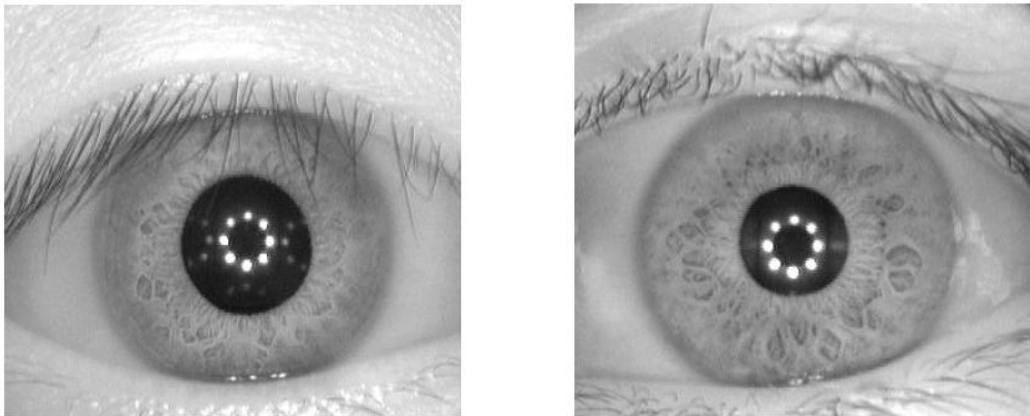


Fig. 7.2: Example iris images in CASIA-Iris-Interval

7.2.2 MMU

MMU1 iris database contributes a total number of 450 iris images (refer to Fig. 7.3) which were taken using LG IrisAccess @2200. This operates at the range of 7-25 cm. On the other hand, MMU2 iris database consists of 995 iris images [94, 95].



Fig.7.3: Example iris images in MMU1 Database

7.2.3 UBIRIS Database

Many iris recognition algorithms achieve almost perfect results even though they operate under advantageous conditions, such as minimal picture noise factors. These settings are difficult to achieve and require a high level of cooperation from the subject, who is subjected to longer and more painful image collection processes. The goal of UBIRIS is related to this point: it provides images with different types of noise, simulating images captured without or with minimal collaboration from the subjects, to become a practical resource for the evaluation and development of robust iris identification methodologies. The UBIRIS database contains 1877 photos that were gathered from 241 individuals over two separate sessions in September 2004 [96, 97]. It is one of the largest publicly accessible and freely available iris databases.

7.3 Inner and Outer Boundary Detection

Fig. 7.4 illustrates the normalization of iris images from three datasets. For each of the datasets; the one original input image is shown, followed by its inner and outer boundary detection, and then its segmented version and finally its normalized version. Three original images from three datasets are shown in Figs. 7.4(a), 7.4(e) and 7.4(i). First of all, Fig. 7.4(a) is one original image from CASIA-Iris-V4 dataset. For the iris image in Fig. 7.4(a), Figs. 7.4(b), 7.4(c) and 7.4(d) represent the corresponding inner and outer boundaries, segmented and normalized versions, respectively. Secondly, Fig. 7.4(e) is one original image from CASIA-Iris-V1 dataset. For the iris image in Fig. 7.4(e), Figs. 7.4(f), 7.4(g), and 7.4(h) represent the corresponding inner and outer boundaries, segmented and normalized versions, respectively. Thirdly, Fig. 7.4(i) is one original image from the MMU iris database and Figs. 7.4(j), 7.4(k) and 7.4(l) represent the corresponding inner and outer boundaries, segmented and normalized versions, respectively.

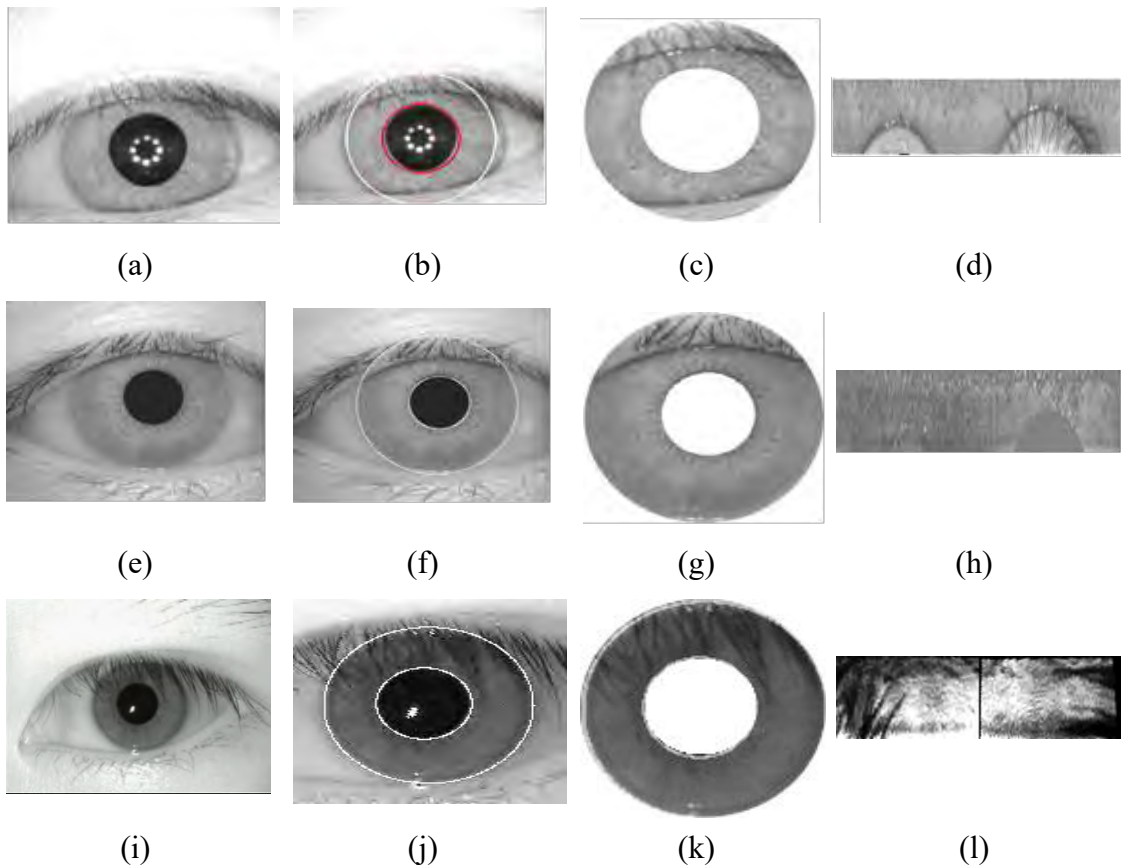


Fig. 7.4: Illustrations of (a, e, i) original input images; (b, f, j) images with inner and outer boundary detection; (c, g, k) segmented iris regions, (d, h, l) iris images after normalization

7.4 Performance Evaluation using Haar wavelet and MLBP

This section discusses the experimental results of the proposed method. For the experimentation, images are obtained from three different datasets [33-35]. Figs. 7.1, 7.2, and 7.3 correspond to images from CASIA-IRIS-V4 [33], CASIA-IRIS-V1 [34], and MMU [35] datasets, respectively. The datasets are described in Table 7.1. CASIA-IRIS-V4 dataset consists of 2639 images of 249 subjects/persons. On the other hand, the CASIA-IRIS-V1 dataset has 756 iris images from 108 eyes of 54 subjects, while the MMU dataset consists of 450 images of 45 subjects. Firstly, one original iris image from [84] is illustrated in Fig. 7.5(a), whereas Fig. 7.5(b) is the corresponding template after applying LBP to LL3 of size 8×64 . For clarity, Fig. 7.5(c) illustrates a larger view of the final template. The template is further reduced to 1×64 size by applying XOR operation through column vectors. Secondly, Figs. 7.6(a), 7.6(b), and 7.6(c) illustrate another original iris image from [87], its corresponding

template after applying LBP, and a larger view of the template, respectively. Thirdly, Figs. 7.7(a), 7.7(b) and 7.7(c) illustrate the same for an original iris image from [95].

Table 7.1: Description of the datasets used in this work

Dataset	Images	Subjects	Sensor	Light wavelength
CASIA-IRIS-V4 (CASIA-Iris-Interval) [84]	2639	249	CASIA close-up iris camera	NIR
CASIA-IRIS-V1 [87]	756	54	CASIA close-up iris camera	NIR
MMU (MMU 1) [95]	450	45	LG EOU 2200	NIR

The performance of the proposed method is evaluated for above mentioned three datasets. For each dataset, 90% (rounded up to the next integer) of the images are considered for training while the remaining are considered for testing.

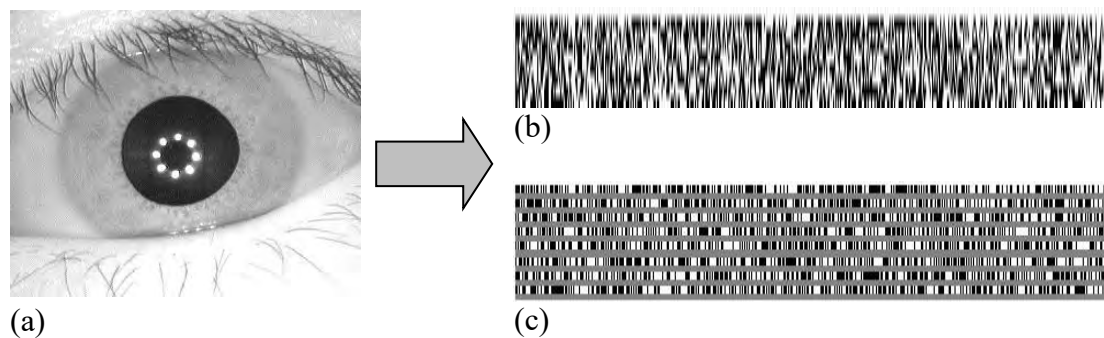


Fig. 7.5: (a) An original iris image from CASIA-IRIS-V4 dataset [84], (b) the final generated iris template, (c) larger view of the binarized template

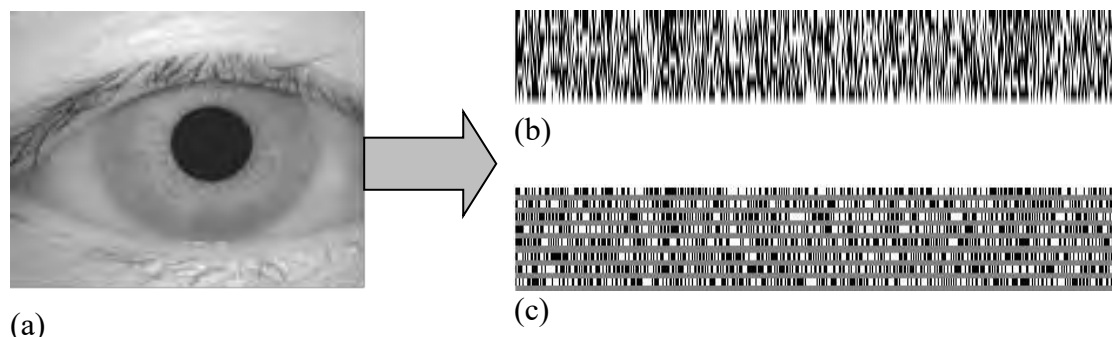


Fig. 7.6: (a) An original iris image from CASIA-IRIS-V1 dataset [87], (b) the final generated iris template, (c) larger view of the binarized template

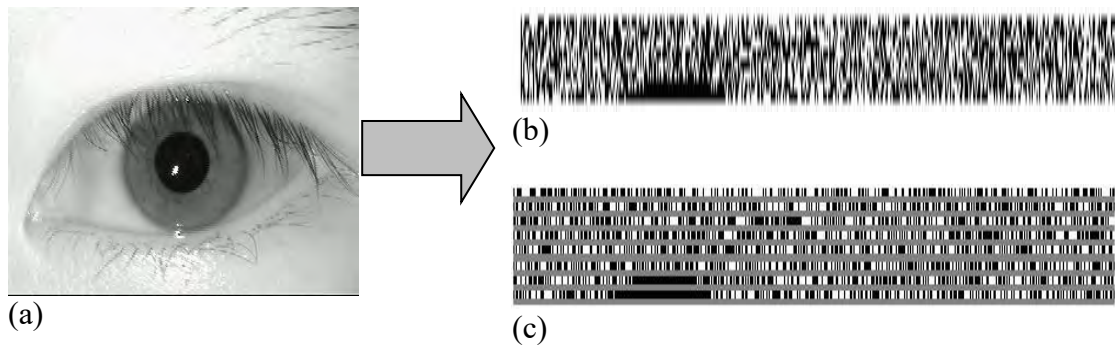


Fig. 7.7. (a) An original iris image from the MMU dataset [95], (b) the final generated iris template, (c) a larger view of the binarized template

Next, the proposed new method is compared with the existing techniques reported in the literature [3], [37, 38], [51], [54]. Table 7.2 presents the comparative results of the proposed method with the previous ones. For the proposed method, the best results that are obtained with Hamming distance method using the CASIA-IRIS-V1 dataset are taken into consideration. In this case, the threshold value is set for computing FAR which is the rate at which a biometric security system incorrectly accepts an unauthorized user and FRR which is the rate at which the system incorrectly rejects an authorized user. In other words, the FAR is the ratio of the *number of false acceptance* (NFA) to the *number of imposter verification attempts* (NIVA), whereas FRR is the ratio of the number of false rejections (NFR) to the number of *enrollee verification attempts* (NEVA). This proposed method and the works in [37, 54] use the same CASIA-IRIS-V1 dataset having BMP images with a resolution of 320×280 . From Table 7.2, it can be seen that the proposed method has a FAR of 0.003% and FRR of 0.80% and an average accuracy of 98.30%. The feature vector length and the computation time of the proposed scheme is significantly lower than existing methods reported in [3], [37, 38], [51], [54]. Among the research works listed in Table 7.2, the proposed method has the second-best (lowest) FAR percentage while the work in [54] reports having a FAR of 0%, but its generated feature vector length is over 8.5 times that of our proposed one. The extremely low FAR (0.003%) attained by our method indicates its strong security capability by not allowing access to imposter iris. As a comparison to the method proposed in [37], which is a highly cited work in this domain, our method outperforms in all three performance metrics with highly reduced feature vector length ($1/24^{\text{th}}$ of the former), making our method highly suitable for real-time person identification. The average accuracy of the proposed scheme is slightly lower than those reported in [38], and [54]. Similarly, the

method in [38], though it produces higher accuracy, suffers from the highest FAR and FRR of all methods, including ours. Considering all performance metrics and very small feature vector, the proposed method is highly attractive for real-time applications.

Table 7.2: Comparisons of results with the existing methods

Reference	Feature Vector length	FAR (in %)	FRR (in %)	Avg. Accuracy (in %)	Dataset	Image Resolution
[37]	1×1536	0.02	1.98	98.00	CASIA-IRIS-V1	BMP format with resolution 320×280
[38]	1×384	0.10	3.56	99.85	CASIA-IRIS-V1	BMP format with resolution 320×280
[54]	1×546	0.00	0.69	99.14	CASIA-IRIS-V1	BMP format with resolution 320×280
Proposed method (Hamming distance)	1×64	0.003	0.80	98.30	CASIA-IRIS-V1	BMP format with resolution 320×280
Proposed method (Hamming distance)	1×64	0.004	0.82	98	CASIA-IRIS-V4	8-bit Gray level JPEG
Proposed method (Hamming distance)	1×64	0.008	0.88	96.80	MMU 1	Greyscale image with resolution 320×240

7.5 Performance Evaluation using LBPX

In this section, we describe the experimental results of the LBPX scheme. For the experimentation, images are obtained from three datasets. There are 1877 images in the UBIRISv1 database collected from 241 persons [96]. This set of iris images enables the recognition techniques because of having several noise factors within the images. There are 2639 images of 249 subjects in the CASIA-IRIS-V4 database [84]. IITD dataset consists of a total of 1120 images collected from 224 users having ages of 14-55 years. Out of 224, 176 users are males, and 48 users are females [86]. Table 7.3 shows the accuracy values of LBPX for three datasets. Table 7.3 indicates that the accuracy value of 97.15% and 97.20% is achieved for the case of CASIA-IRIS-V4 and CASIA-IRIS-V4 datasets, respectively. In addition, IITD has an accuracy of 96.40%, while UBIRIS has 96% accuracy.

Table 7.3: Comparison of accuracy of proposed LBPX

Dataset	Successful Matching Rate using HD
CASIA-IRIS-V1	97.15%
CASIA-IRIS-V4	97.20%
UBIRIS	96%
IITD	96.40%

Table 7.4: Comparative analysis between LBPX and other methods

Reference	Size of Feature Vector	No. of times higher than the proposed method	Overall Recognition Accuracy
[77]	1x384	48	99.85%
[44]	1x1536	192	98%
[83]	1x400	50	90.34%
[31]	1x200	25	98.63%
[31]	1x1000	125	96.56%
[40]	1x992	124	86.53%
RIU LBP (Q=24, R=3)	1x26	3.25	97.20%
RIU LBP (Q=16, R=2)	1x18	2.25	96.60%
LBPX	1x8	-	97.15%

Table 7.4 shows the comparative summary of LBPX and existing methods. CASIA Iris-V1 dataset was used in [31]. CASIA Iris-V4 dataset was used in [44, 77, 83]. In Table 7.4, the size of the feature vectors and the recognition accuracy is shown for different studies. Results show that the work in [77] results in a feature vector size of 1x384 at an accuracy of 99.85%. The performance of RIU LBP was also evaluated. It was found that RIU LBP (Q=24, R=3) achieved a vector size of 1x26 at an accuracy of 97.20%, while RIU LBP (Q=16, R=2) exhibited a vector size of 1x18 at an accuracy of 96.60%. On the other hand, the proposed LBPX has a reduced feature vector size of only 1x8 at an accuracy of 96.40%. Therefore, LBPX outperforms others in terms of reduced feature vector size.

CHAPTER 8

Conclusion and Future Works

8.1 Summary of the Work

This thesis has presented an iris recognition system and two algorithms for iris feature reduction.

Firstly, an iris recognition method is presented using an efficient iris feature extraction for the selection of optimal features with reduced feature-length. Firstly, the Haar wavelet is applied to the normalized iris. The three-level Haar wavelet decomposition produces LL3 (level-3 approximation part) which is considered as a major characteristics region. A similar approach has been utilized for local binary pattern feature extraction used in the approach. LBP operators cannot properly detect large-scale textural structures. To overcome this problem, this feature extraction scheme has been applied to LL3 part, and reduced feature-length has been obtained. Secondly, a novel LBP method termed LBPX is proposed in order to reduce the size of the iris feature vector more. Different types of rotation invariant LBP has been applied and compared to LBPX for different iris databases. Results show that the proposed methods reduce the feature-length multiple times than the existing methods reported in the literature. This reduced length results in a reduction in computation time. This reduced feature-length is at the cost of a small amount of reduction in the accuracy level compared with some previously proposed methods but still produces better FAR and FRR than existing methods. Hence, the proposed two methods are highly attractive to develop a fast and reliable iris recognition system.

8.2 Main Findings of the Work

At the feature extraction stage, the proposed methods considerably reduce the computation time and also shrink the feature-length without loss of major information of the characteristics region. It is proposed in this thesis that a novel hybrid HWT and MLBP-based technique be developed to reduce feature size in order to match iris pictures more quickly. The most notable features of the iris are extracted using HWT, which reduces the template size. In this study, a three-level HWT is used to extract

the region of the iris picture that contains the majority of the important information. It is deemed to be a major characteristics region when the three-level approximation part derived from HWT is evaluated. The repeated HWT, for example, changes a 64×512 normalized iris picture into an approximation image of 8×64 , which after application of MLBP and XOR becomes a template of 1×64 following the application of MLBP. On three independent iris datasets, the suggested hybrid HWT and MLBP methods are tested and proven to be effective. Using the proposed method, the feature-length is reduced by multiple orders of magnitude compared to the existing methods reported in the literature, according to the results. As a result of the shorter length, the computation time is shorter as well.

A new form of the local binary pattern (LBP) termed LBPX is proposed in this thesis as an iris feature extraction method. In this LBPX, we combine the concepts of uniform LBP, rotation-invariant LBP, and an XOR approach followed by LBP operations to create a hybrid of these concepts. Comparing the suggested technique to current methods, such as RIU LBP, the new method results in a reduced feature vector size. It is possible to attain an acceptable accuracy with a 1×8 feature vector size when used to the CASIA, UBIRIS, and IITD datasets. The performance of LBPX based recognition system adopting iris image is evaluated in terms of accuracy and feature vector length. Furthermore, results show LBPX outperforms existing feature extraction methods in terms of reduced feature-length, ensuring faster iris recognition. This reduced length can definitely improve speed. The proposed approaches can be further improved by proper iris segmentation with removing image artefacts. However, this proposed approach is effective enough to be used with a security system where a higher speed of recognition rate is required with more accuracy.

8.3 Suggestions for Future Work

In this thesis, the proposed approaches perform reasonably well. However, there are a number of issues, which should be addressed and resolved. In order to increase the accuracy of the system, a more accurate and elaborate eyelids and eyelashes detection scheme can be employed. Since the quality of the images affects the overall matching accuracy, an iris quality assessment scheme can be deployed. The most complex part involves the feature extraction and size of feature vector reduction with HWT and MLBP maintaining good recognition accuracy. Since the system has been

implemented in MATLAB, which is an interpreted language, development of speed can be achieved if the most time-consuming part is implemented in C or C++. Traditional Hamming Distance and Euclidean distance have been used for the classification of iris templates. A more accurate classifier can be used for better classification. In the future, Artificial Neural Network strategies such as deep learning can be employed to reduce the computational time for the overall iris recognition system. In order to make the proposed approach applicable in real-time situations, reducing the overall time consumption may be considered an important factor. Many efficient systems for iris recognition are available nowadays. However, the properties of iris texture and the underlying processes of generating it have not been explored. Therefore, an additional room for the extension of the successful iris recognition system is to give an insight into these aspects.

Although the experimental results exhibit that the proposed approaches work well, there are still some anomalies that should be considered. The iris liveness detection is a major issue in this respect. Fake iris detection is another important factor that should be handled carefully. Contact lenses are vastly used nowadays, which can change the individual's iris recognition accuracy. They may create a problem for any iris recognition system. Furthermore, spectacles may introduce too much specular reflection, which results in failure of automatic segmentation or recognition.

References

- [1] Nguyen, K., Fookes, C., Jillela, R., Sridharan, S., and Ross, A., "Long range iris recognition: A survey," *Pattern Recognition*, vol. 72, pp. 123-143, 2017.
- [2] Bhatia, R., "Biometrics and face recognition techniques," *International Journal of Advanced Research in Computer Science and Software Engineering*, vol. 3, no. 5, 2013.
- [3] Daugman, J. G., "High confidence visual recognition of persons by a test of statistical independence," *IEEE transactions on pattern analysis and machine intelligence*, vol. 15, no. 11, pp. 1148-1161, 1993.
- [4] Daugman, J. G., "Biometric personal identification system based on iris analysis," Google Patents, 1994.
- [5] Daugman, J., "How iris recognition works," *IEEE Transactions on Circuits and Systems for Video Technology*, vol. 14, no. 1, pp. 21-30, 2004.
- [6] Boles, W. W., and Boashash, B., "A human identification technique using images of the iris and wavelet transform," *IEEE transactions on signal processing*, vol. 46, no. 4, pp. 1185-1188, 1998.
- [7] Daugman, J., "Statistical richness of visual phase information: update on recognizing persons by iris patterns," *International Journal of computer vision*, vol. 45, no. 1, pp. 25-38, 2001.
- [8] Tisse, C.-l., Martin, L., Torres, L., and Robert, M., "Person identification technique using human iris recognition," in *The 15th International Conference on Vision Interface*, 2002, pp. 294-299.
- [9] Daugman, J., "New methods in iris recognition," *IEEE Transactions on Systems, Man, and Cybernetics, Part B (Cybernetics)*, vol. 37, no. 5, pp. 1167-1175, 2007.
- [10] Kumar, D. R. S., Raja, K. B., Nuthan, N., Sindhuja, B., Supriya, P., Chhotaray, R. K., and Pattnaik, S., "Iris recognition based on DWT and PCA," in *2011 International Conference on Computational Intelligence and Communication Networks*, 2011, pp. 489-493.
- [11] Alim, O. A., and Sharkas, M., "Iris recognition using discrete wavelet transform and artificial neural networks." pp. 337-340.
- [12] Liam, L. W., Chekima, A., Fan, L. C., and Dargham, J. A., "Iris recognition using self-organizing neural network," in *Student conference on research and development*, 2002, pp. 169-172.
- [13] Liu, X., Bowyer, K. W., and Flynn, P. J., "Experiments with an improved iris segmentation algorithm." pp. 118-123.
- [14] Liu, X., Bowyer, K. W., and Flynn, P. J., "Experimental evaluation of iris recognition." pp. 158-158.
- [15] Trucco, E., and Razeto, M., "Robust iris location in close-up images of the eye," *Pattern analysis and applications*, vol. 8, no. 3, pp. 247-255, 2005.
- [16] Huang, P. S., Chiang, C.-S., and Liang, J.-R., "Iris recognition using Fourier-wavelet features." pp. 14-22.
- [17] Feng, X., Fang, C., Ding, X., and Wu, Y., "Iris localization with dual coarse-to-fine strategy." pp. 553-556.
- [18] Zhang, W., Li, B., Ye, X., and Zhuang, Z., "A robust algorithm for iris localization based on radial symmetry." pp. 324-327.
- [19] Luengo-Oroz, M. A., Faure, E., and Angulo, J., "Robust iris segmentation on uncalibrated noisy images using mathematical morphology," *Image and Vision Computing*, vol. 28, no. 2, pp. 278-284, 2010.

- [20] Kong, W.-K., and Zhang, D., "Detecting eyelash and reflection for accurate iris segmentation," *International journal of pattern recognition and artificial intelligence*, vol. 17, no. 06, pp. 1025-1034, 2003.
- [21] Zhou, Z., Du, Y., and Belcher, C., "Transforming traditional iris recognition systems to work in nonideal situations," *IEEE Transactions on Industrial Electronics*, vol. 56, no. 8, pp. 3203-3213, 2009.
- [22] Sun, Z., Wang, Y., Tan, T., and Cui, J., "Improving iris recognition accuracy via cascaded classifiers," *IEEE Transactions on Systems, Man, and Cybernetics, Part C (Applications and Reviews)*, vol. 35, no. 3, pp. 435-441, 2005.
- [23] He, Z., Tan, T., and Sun, Z., "Iris localization via pulling and pushing." pp. 366-369.
- [24] Proenca, H., "Iris recognition: On the segmentation of degraded images acquired in the visible wavelength," *IEEE Transactions on Pattern Analysis and Machine Intelligence*, vol. 32, no. 8, pp. 1502-1516, 2009.
- [25] Proença, H., and Alexandre, L. A., "Toward noncooperative iris recognition: A classification approach using multiple signatures," *IEEE transactions on pattern analysis and machine intelligence*, vol. 29, no. 4, pp. 607-612, 2007.
- [26] Kronfeld, P. C., "The gross anatomy and embryology of the eye," *Vegetative Physiology and Biochemistry*, pp. 1-62: Elsevier, 1962.
- [27] Chedekel, M. R., "Photophysics and photochemistry of melanin." pp. 264-264.
- [28] Daugman, J., "Iris recognition: The colored part of the eye contains delicate patterns that vary randomly from person to person, offering a powerful means of identification," *American scientist*, vol. 89, no. 4, pp. 326-333, 2001.
- [29] Tan, C.-W., and Kumar, A., "Unified framework for automated iris segmentation using distantly acquired face images," *IEEE Transactions on Image Processing*, vol. 21, no. 9, pp. 4068-4079, 2012.
- [30] Zuo, J., and Schmid, N. A., "On a methodology for robust segmentation of nonideal iris images," *IEEE Transactions on Systems, Man, and Cybernetics, Part B (Cybernetics)*, vol. 40, no. 3, pp. 703-718, 2009.
- [31] Masek, L., "Recognition of human iris patterns for biometric identification," *Bachelor's Thesis, University of Western Australia*, 2003.
- [32] Daugman, J., "The importance of being random: statistical principles of iris recognition," *Pattern recognition*, vol. 36, no. 2, pp. 279-291, 2003.
- [33] Khan, T. Z., Podder, P., and Hossain, M. F., "Fast and efficient iris segmentation approach based on morphology and geometry operation," in *The 8th International Conference on Software, Knowledge, Information Management and Applications (SKIMA 2014)*, Dhaka, 2014, pp. 1-8.
- [34] Wildes, R. P., Asmuth, J. C., Hanna, K. J., Hsu, S. C., Kolczynski, R. J., Matey, J. R., and McBride, S. E., *Automated, non-invasive iris recognition system and method*, to Google Patents, 1996.
- [35] Flom, L., and Safir, A., "Iris recognition system, United States Patent, US 4641349," 1987.
- [36] Daugman, J., and Downing, C., "Epigenetic randomness, complexity and singularity of human iris patterns," *Proceedings of the Royal Society of London. Series B: Biological Sciences*, vol. 268, no. 1477, pp. 1737-1740, 2001.
- [37] Ma, L., Tan, T., Wang, Y., and Zhang, D., "Personal identification based on iris texture analysis," *IEEE transactions on pattern analysis and machine intelligence*, vol. 25, no. 12, pp. 1519-1533, 2003.

- [38] Ma, L., Wang, Y., and Tan, T., "Iris recognition using circular symmetric filters," in *2002 International Conference on Pattern Recognition*, 2002, pp. 414-417.
- [39] Monroe, D. M., Rakshit, S., and Zhang, D., "DCT-based iris recognition," *IEEE transactions on pattern analysis and machine intelligence*, vol. 29, no. 4, pp. 586-595, 2007.
- [40] Li, X., Jiang, Y., Chen, M., and Li, F., "Research on iris image encryption based on deep learning," *EURASIP Journal on Image and Video Processing*, vol. 2018, no. 1, pp. 1-10, 2018.
- [41] Umer, S., Dhara, B. C., and Chanda, B., "Texture code matrix-based multi-instance iris recognition," *Pattern Analysis and Applications*, vol. 19, no. 1, pp. 283-295, 2016.
- [42] Soliman, R. F., Amin, M., and Abd El-Samie, F. E., "A Novel Cancelable Iris Recognition Approach." pp. 359-368.
- [43] Ahmadi, N., and Akbarizadeh, G., "Hybrid robust iris recognition approach using iris image pre-processing, two-dimensional gabor features and multi-layer perceptron neural network/PSO," *Iet Biometrics*, vol. 7, no. 2, pp. 153-162, 2018.
- [44] Barpanda, S. S., Majhi, B., Sa, P. K., Sangaiah, A. K., and Bakshi, S., "Iris feature extraction through wavelet mel-frequency cepstrum coefficients," *Optics & Laser Technology*, vol. 110, pp. 13-23, 2019.
- [45] Barpanda, S. S., Sa, P. K., Marques, O., Majhi, B., and Bakshi, S., "Iris recognition with tunable filter bank based feature," *Multimedia Tools and Applications*, vol. 77, no. 6, pp. 7637-7674, 2018.
- [46] Alvarez-Betancourt, Y., and Garcia-Silvente, M., "A keypoints-based feature extraction method for iris recognition under variable image quality conditions," *Knowledge-Based Systems*, vol. 92, pp. 169-182, 2016.
- [47] Seetharaman, K., and Ragupathy, R., "LDPC and SHA based iris recognition for image authentication," *Egyptian Informatics Journal*, vol. 13, no. 3, pp. 217-224, 2012.
- [48] Sahu, B., Sa, P. K., Bakshi, S., and Sangaiah, A. K., "Reducing dense local feature key-points for faster iris recognition," *Computers & Electrical Engineering*, vol. 70, pp. 939-949, 2018.
- [49] Jamaludin, S., Zainal, N., and Zaki, W., "Sub-iris Technique for Non-ideal Iris Recognition," *Arabian Journal for Science & Engineering (Springer Science & Business Media BV)*, vol. 43, no. 12, 2018.
- [50] Dhage, S. S., Hegde, S. S., Manikantan, K., and Ramachandran, S., "DWT-based feature extraction and radon transform based contrast enhancement for improved iris recognition," *Procedia Computer Science*, vol. 45, pp. 256-265, 2015.
- [51] de Martin-Roche, D., Sanchez-Avila, C., and Sanchez-Reillo, R., "Iris recognition for biometric identification using dyadic wavelet transform zero-crossing." pp. 272-277.
- [52] Bakshi, S., Sa, P. K., and Majhi, B., "A novel phase-intensive local pattern for periocular recognition under visible spectrum," *Biocybernetics and Biomedical Engineering*, vol. 35, no. 1, pp. 30-44, 2015.
- [53] Nigam, A., Kumar, B., Triyar, J., and Gupta, P., "Iris recognition using discrete cosine transform and relational measures." pp. 506-517.
- [54] Te Chu, C., and Chen, C.-H., "High performance iris recognition based on LDA and LPCC." pp. 5-pp.

- [55] Zahran, B., Al-Azzeh, J., Alqadi, Z., Al-Zoghoul, M.-A., and Khawatreh, S., "A MODIFIED LBP METHOD TO EXTRACT FEATURES FROM COLOR IMAGES," *Journal of Theoretical & Applied Information Technology*, vol. 96, no. 10, 2018.
- [56] Miyazawa, K., Ito, K., Aoki, T., Kobayashi, K., and Nakajima, H., "An effective approach for iris recognition using phase-based image matching," *IEEE transactions on pattern analysis and machine intelligence*, vol. 30, no. 10, pp. 1741-1756, 2008.
- [57] Llano, E. G., García-Vázquez, M. S., Zamudio-Fuentes, L. M., Vargas, J. M. C., and Ramírez-Acosta, A. A., "Analysis of the improvement on textural information in human iris recognition." pp. 373-376.
- [58] Kumar, S., Singh, S., and Kumar, J., "Automatic live facial expression detection using genetic algorithm with haar wavelet features and SVM," *Wireless Personal Communications*, vol. 103, no. 3, pp. 2435-2453, 2018.
- [59] Khan, S. A., Ishtiaq, M., Nazir, M., and Shaheen, M., "Face recognition under varying expressions and illumination using particle swarm optimization," *Journal of computational science*, vol. 28, pp. 94-100, 2018.
- [60] Owusu, E., Abdulai, J. D., and Zhan, Y., "Face detection based on multilayer feed-forward neural network and Haar features," *Software: Practice and Experience*, vol. 49, no. 1, pp. 120-129, 2019.
- [61] Bhattacharjee, D., Seal, A., Ganguly, S., Nasipuri, M., and Basu, D. K., "A comparative study of human thermal face recognition based on Haar wavelet transform and local binary pattern," *Computational intelligence and neuroscience*, vol. 2012.
- [62] Shaju, S., and Davis, D., "Haar wavelet transform based histogram concatenation model for finger print spoofing detection." pp. 1352-1356.
- [63] Ahmadi, N., and Nilashi, M., "Iris texture recognition based on multilevel 2-D Haar wavelet decomposition and Hamming distance approach," *Journal of Soft Computing and Decision Support Systems*, vol. 5, no. 3, pp. 16-20, 2018.
- [64] Oktiana, M., Saddami, K., Arnia, F., Away, Y., Hirai, K., Horiuchi, T., and Munadi, K., "Advances in cross-spectral iris recognition using integrated gradientface-based normalization," *IEEE Access*, vol. 7, pp. 130484-130494, 2019.
- [65] Shuai, L., Yuanning, L., Xiaodong, Z., Guang, H., Jingwei, C., Qixian, Z., Zukang, W., Xinlong, L., and Chaoqun, W., "Multi-source feature fusion and entropy feature lightweight neural network for constrained multi-state heterogeneous iris recognition," *IEEE Access*, vol. 8, pp. 53321-53345, 2020.
- [66] Ahmadi, N., Nilashi, M., Samad, S., Rashid, T. A., and Ahmadi, H., "An intelligent method for iris recognition using supervised machine learning techniques," *Optics & Laser Technology*, vol. 120, pp. 105701, 2019.
- [67] Chen, Y., Wu, C., and Wang, Y., "T-center: a novel feature extraction approach towards large-scale iris recognition," *IEEE Access*, vol. 8, pp. 32365-32375, 2020.
- [68] Rana, H. K., Azam, M. S., Akhtar, M. R., Quinn, J. M. W., and Moni, M. A., "A fast iris recognition system through optimum feature extraction," *PeerJ Computer Science*, vol. 5, pp. e184, 2019.
- [69] Huo, G., Guo, H., Zhang, Y., Zhang, Q., Li, W., and Li, B., "An effective feature descriptor with Gabor filter and uniform local binary pattern transcoding for Iris recognition," *Pattern Recognition and Image Analysis*, vol. 29, no. 4, pp. 688-694, 2019.

- [70] Ahmadi, N., "Morphological-edge detection approach for the human iris segmentation," *Journal of Soft Computing and Decision Support Systems*, vol. 6, no. 4, pp. 15-19, 2019.
- [71] Winston, J. J., and Hemanth, D. J., "Performance Comparison of Feature Extraction Methods for Iris Recognition," *Information Technology and Intelligent Transportation Systems*, vol. 323, pp. 62, 2020.
- [72] Danlami, M., Jamel, S., Ramli, S. N., and Azahari, S. R. M., "Comparing the Legendre Wavelet filter and the Gabor Wavelet filter For Feature Extraction based on Iris Recognition System," in *2020 IEEE 6th International Conference on Optimization and Applications (ICOA)*, 2020, pp. 1-6.
- [73] Vyas, R., Kanumuri, T., and Sheoran, G., "Cross spectral iris recognition for surveillance based applications," *Multimedia Tools and Applications*, vol. 78, no. 5, pp. 5681-5699, 2019.
- [74] Noruzi, A., Mahlouji, M., and Shahidinejad, A., "Robust iris recognition in unconstrained environments," *Journal of AI and Data Mining*, vol. 7, no. 4, pp. 495-506, 2019.
- [75] Chen, X.-h., Wang, J.-s., Ruan, Y.-l., and Gao, S.-z., "An Improved Iris Recognition Method Based on Discrete Cosine Transform and Gabor Wavelet Transform Algorithm," *Engineering Letters*, vol. 27, no. 4, 2019.
- [76] Abdalla, M. A. E., Abdo, A. A., and Lawgali, A. O., "Utilizing Discrete Wavelet Transform and Discrete Cosine Transform for Iris Recognition," in *20th International Conference on Sciences and Techniques of Automatic Control and Computer Engineering (STA)*, 2020, pp. 283-286.
- [77] Wang, Y., and Zheng, H., "An Improved Iris Recognition Method Based on Wavelet Packet Transform," in *International Conference on Mechanical Automation and Computer Engineering (MACE 2020)*, 2020, pp. 042239.
- [78] Rafik, H. D., and Boubaker, M., "Application of metaheuristic for optimization of iris Image segmentation by using evaluation Hough Transform and methods Daugman," in *1st International Conference on Communications, Control Systems and Signal Processing (CCSSP)*, 2020, pp. 142-150.
- [79] Abdo, A. A., Lawgali, A., and Zohdy, A. K., "Iris recognition based on histogram equalization and discrete cosine transform," in *The 6th International Conference on Engineering & MIS 2020*, 2020, pp. 1-5.
- [80] Kyaw, T., Tun, P. T., and Swe, K. T., "PERFORMANCE ANALYSIS OF FEATURES EXTRACTION ON IRIS RECOGNITION SYSTEM," *International Journal Of All Research Writings*, vol. 2, no. 12, pp. 99-107, 2020.
- [81] Adamović, S., Mišković, V., Maček, N., Milosavljević, M., Šarac, M., Saračević, M., and Gnjatović, M., "An efficient novel approach for iris recognition based on stylometric features and machine learning techniques," *Future Generation Computer Systems*, vol. 107, pp. 144-157, 2020.
- [82] Danlami, M., Jamel, S., Ramli, S. N., and Azahari, S. R. M., "Comparing the Legendre Wavelet filter and the Gabor Wavelet filter For Feature Extraction based on Iris Recognition System," in *IEEE 6th International Conference on Optimization and Applications (ICOA)*, 2020, pp. 1-6.
- [83] Ali, L. E., Luo, J., and Ma, J., "Effective Iris Recognition for Distant Images Using Log-Gabor Wavelet Based Contourlet Transform Features," *Intelligent Computing Theories and Application*. pp. 293-303.
- [84] "Institute of Automation, Chinese Academy of Science: CASIA v4.0 Iris Image Database," 2008.

- [85] Abikoye, O. C., Aro, T. O., Ogundokun, O., and Akande, H. B., "Comparative Analysis of Selected Feature Extraction Techniques for Iris Recognition System," *FUW Trends in Science & Technology Journal*, vol. 3, no. 2A, pp. 541-545, 2019.
- [86] "IIT Delhi Iris Database (Version 1.0)," Delhi, ed., 2007.
- [87] "Institute of Automation, Chinese Academy of Science: CASIA v1.0 Iris Image Database," 2008.
- [88] Podder, P., Parvez, A. H. M. S., Yeasmin, M. N., and Khalil, M. I., "Relative performance analysis of edge detection techniques in iris recognition system," in *2018 International Conference on Current Trends towards Converging Technologies (ICCTCT)*, 2018, pp. 1-6.
- [89] Bharati, S., Khan, T. Z., Podder, P., and Hung, N. Q., "A Comparative Analysis of Image Denoising Problem: Noise Models, Denoising Filters and Applications," *Cognitive Internet of Medical Things for Smart Healthcare: Services and Applications*, Hassanien, Khamparia, Gupta, Shankar and Slowik, eds., pp. 49-66, Cham: Springer International Publishing, 2021.
- [90] Ojala, T., Pietikäinen, M., and Mäenpää, T., "Gray Scale and Rotation Invariant Texture Classification with Local Binary Patterns," *Computer Vision - ECCV 2000*. pp. 404-420.
- [91] Ojala, T., Pietikäinen, M., and Maenpaa, T., "Multiresolution gray-scale and rotation invariant texture classification with local binary patterns," *IEEE Transactions on pattern analysis and machine intelligence*, vol. 24, no. 7, pp. 971-987, 2002.
- [92] Ojala, T., Pietikäinen, M., and Mäenpää, T., "A Generalized Local Binary Pattern Operator for Multiresolution Gray Scale and Rotation Invariant Texture Classification," *Advances in Pattern Recognition — ICAPR 2001*. pp. 399-408.
- [93] SORIANO, M., OJALA, T., and PIETIKÄINEN, M., "ROBUSTNESS OF LOCAL BINARY PATTERN (LBP) OPERATORS TO TILT-COMPENSATED TEXTURES," *Texture Analysis in Machine Vision*, pp. 89-99.
- [94] Woodard, D. L., and Ricanek, K., "Iris Databases," *Encyclopedia of Biometrics*, Li and Jain, eds., pp. 770-774, Boston, MA: Springer US, 2009.
- [95] "Multimedia University: MMU1 and MMU2 Iris Image Databases," 2008.
- [96] Proença, H., and Alexandre, L. A., "UBIRIS: A Noisy Iris Image Database," *Image Analysis and Processing – ICIAP 2005*. pp. 970-977.
- [97] Proenca, H., and Alexandre, L. A., "Iris recognition: Measuring feature's quality for the feature selection in unconstrained image capture environments," in *2006 IEEE International Conference on Computational Intelligence for Homeland Security and Personal Safety*, 2006, pp. 35-40.